

Rowan University

Rowan Digital Works

Rowan-Virtua School of Osteopathic Medicine
Faculty Scholarship

Rowan-Virtua School of Osteopathic Medicine

2-2024

Ksp1 Is an Autophagic Receptor Protein for the Snx4-Assisted Autophagy of Ssn2/Med13

Sara E Hanley
Rowan University

Stephen D Willis
Rowan University

Steven J Doyle
Rowan University

Randy Strich
Rowan University

Katrina F Cooper
Rowan University

Follow this and additional works at: https://rdw.rowan.edu/som_facpub

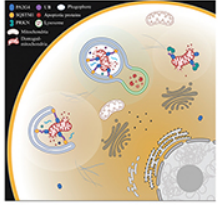


Part of the [Cell Biology Commons](#), [Laboratory and Basic Science Research Commons](#), [Medical Molecular Biology Commons](#), and the [Molecular Biology Commons](#)

Recommended Citation

Hanley, Sara E; Willis, Stephen D; Doyle, Steven J; Strich, Randy; and Cooper, Katrina F, "Ksp1 Is an Autophagic Receptor Protein for the Snx4-Assisted Autophagy of Ssn2/Med13" (2024). *Rowan-Virtua School of Osteopathic Medicine Faculty Scholarship*. 193.
https://rdw.rowan.edu/som_facpub/193

This Article is brought to you for free and open access by the Rowan-Virtua School of Osteopathic Medicine at Rowan Digital Works. It has been accepted for inclusion in Rowan-Virtua School of Osteopathic Medicine Faculty Scholarship by an authorized administrator of Rowan Digital Works.



Ksp1 is an autophagic receptor protein for the Snx4-assisted autophagy of Ssn2/Med13

Sara E. Hanley, Stephen D. Willis, Steven J. Doyle, Randy Strich & Katrina F. Cooper

To cite this article: Sara E. Hanley, Stephen D. Willis, Steven J. Doyle, Randy Strich & Katrina F. Cooper (2024) Ksp1 is an autophagic receptor protein for the Snx4-assisted autophagy of Ssn2/Med13, *Autophagy*, 20:2, 397-415, DOI: [10.1080/15548627.2023.2259708](https://doi.org/10.1080/15548627.2023.2259708)

To link to this article: <https://doi.org/10.1080/15548627.2023.2259708>



© 2023 The Author(s). Published by Informa UK Limited, trading as Taylor & Francis Group.



[View supplementary material](#)



Published online: 25 Jan 2024.



[Submit your article to this journal](#)



Article views: 708



[View related articles](#)



[View Crossmark data](#)

Ksp1 is an autophagic receptor protein for the Snx4-assisted autophagy of Ssn2/Med13

Sara E. Hanley^a, Stephen D. Willis^a, Steven J. Doyle^{a,b}, Randy Strich^a, and Katrina F. Cooper^a 

^aDepartment of Molecular Biology, Rowan-Virtua School of Translational Biomedical Engineering & Sciences, Rowan University, Stratford, NJ, USA;

^bSchool of Osteopathic Medicine, Rowan University, Stratford, NJ, USA

ABSTRACT

Ksp1 is a casein II-like kinase whose activity prevents aberrant macroautophagy/autophagy induction in nutrient-rich conditions in yeast. Here, we describe a kinase-independent role of Ksp1 as a novel autophagic receptor protein for Ssn2/Med13, a known cargo of Snx4-assisted autophagy of transcription factors. In this pathway, a subset of conserved transcriptional regulators, Ssn2/Med13, Rim15, and Msn2, are selectively targeted for vacuolar proteolysis following nitrogen starvation, assisted by the sorting nexin heterodimer Snx4-Atg20. Here we show that phagophores also engulf Ksp1 alongside its cargo for vacuolar proteolysis. Ksp1 directly associates with Atg8 following nitrogen starvation at the interface of an Atg8-family interacting motif (AIM)/LC3-interacting region (LIR) in Ksp1 and the LIR/AIM docking site (LDS) in Atg8. Mutating the LDS site prevents the autophagic degradation of Ksp1. However, deletion of the C terminal canonical AIM still permitted Ssn2/Med13 proteolysis, suggesting that additional non-canonical AIMS may mediate the Ksp1-Atg8 interaction. Ksp1 is recruited to the perivacuolar phagophore assembly site by Atg29, a member of the trimeric scaffold complex. This interaction is independent of Atg8 and Snx4, suggesting that Ksp1 is recruited early to phagophores, with Snx4 delivering Ssn2/Med13 thereafter. Finally, normal cell survival following prolonged nitrogen starvation requires Ksp1. Together, these studies define a kinase-independent role for Ksp1 as an autophagic receptor protein mediating Ssn2/Med13 degradation. They also suggest that phagophores built by the trimeric scaffold complex are capable of receptor-mediated autophagy. These results demonstrate the dual functionality of Ksp1, whose kinase activity prevents autophagy while it plays a scaffolding role supporting autophagic degradation.

Abbreviations: 3-AT: 3-aminotriazole; 17C: Atg17-Atg31-Atg29 trimeric scaffold complex; AIM: Atg8-family interacting motif; ATG: autophagy related; CKM: CDK8 kinase module; Cvt: cytoplasm-to-vacuole targeting; IDR: intrinsically disordered region; LIR: LC3-interacting region; LDS: LIR/AIM docking site; MoRF: molecular recognition feature; NPC: nuclear pore complex; PAS: phagophore assembly site; PKA: protein kinase A; RBP: RNA-binding protein; UPS: ubiquitin-proteasome system. SAA-TF: Snx4-assisted autophagy of transcription factors; Y2H: yeast two-hybrid.

ARTICLE HISTORY

Received 31 January 2023

Revised 7 September 2023

Accepted

11 September 2023

KEYWORDS

Atg8; Ksp1; phagophore assembly site (PAS); receptor proteins; Ssn2/Med13; trimeric scaffold complex (17C)

Introduction

It is well established that maintaining protein homeostasis is essential in preserving normal cellular function. Macroautophagy (hereafter autophagy) is a highly conserved catabolic process that promotes homeostasis [1,2]. As such, autophagy is protective against various diseases, including neurodegeneration, cancer, infections, and cardiovascular disorders [3–5]. Autophagy recycles intracellular material sequestered by the double membrane of autophagosomes. The cargo is delivered to vacuoles (in yeast and plants) or lysosomes (in metazoans) by fusion of the outer autophagosomal membrane with vacuoles. Thereafter, the inner structure, an autophagic body, is released into the vacuolar lumen and degraded by resident hydrolases [6,7]. Depending on the cargo, cytoplasmic material is recycled by either bulk (nonselective) or selective autophagy

pathways. In bulk autophagy, growing phagophores capture portions of the cytoplasm indiscriminately. The phagophore assembly site (PAS) is built on the outer vacuolar membrane and is seeded by the constitutive Atg17 scaffold complex (Atg29, Atg31, and Atg17) [8]. Starvation-induced inactivation of the TORC1 pathway triggers bulk autophagy [9], leading to the upregulation of genes required to execute the autophagy signaling cascade. In *Saccharomyces cerevisiae*, the model organism used in the current study, many of the ATG (autophagy related) genes identified to date are highly conserved [2,10].

By contrast, selective autophagy is active in both physiological and stress conditions, being required to maintain the number and integrity of cellular organelles and protect cells from pathogen invasions [2,11,12]. Two unifying concepts define selective autophagy. First, the process utilizes a receptor protein that links

CONTACT Katrina F. Cooper  cooperka@rowan.edu  Department of Molecular Biology, Rowan-Virtua School of Translational Biomedical Engineering & Sciences, Rowan University, Stratford, NJ 08084, USA

 Supplemental data for this article can be accessed online at <https://doi.org/10.1080/15548627.2023.2259708>

© 2023 The Author(s). Published by Informa UK Limited, trading as Taylor & Francis Group.

This is an Open Access article distributed under the terms of the Creative Commons Attribution-NonCommercial-NoDerivatives License (<http://creativecommons.org/licenses/by-nc-nd/4.0/>), which permits non-commercial re-use, distribution, and reproduction in any medium, provided the original work is properly cited, and is not altered, transformed, or built upon in any way. The terms on which this article has been published allow the posting of the Accepted Manuscript in a repository by the author(s) or with their consent.

cargo to the autophagy machinery through interaction with Atg8 (Atg8 in plants and yeast, LC3/GABARAP in mammals) [2,13–16]. Second, phagophore membrane expansion occurs along the surface of degradation targets mediated by receptor proteins binding to the Atg11 scaffold [17,18]. In yeast, an exception to this is the Cue5 receptor that targets aggregated proteins and dysfunctional proteasomes [19,20].

Recently we defined a new autophagy mechanism [21], coined Snx4-assisted autophagy of transcription factors (SAA-TF). SAA-TF targets transcriptional regulators that both positively (Msn2 and Rim15) and negatively (Ssn2/Med13) regulate *ATG* transcription. Ssn2/Med13, the focus of this current

paper, is a conserved member of the Cdk8 kinase module (CKM) that in yeast predominantly negatively regulates the transcription of stress response genes, including *ATG8* [21–23]. Following nitrogen starvation, removing the CKM from the mediator contributes to *ATG8* upregulation. This is mediated by the vacuolar degradation of Ssn2/Med13 [21] alongside the UPS-mediated destruction of Ssn8/cyclin C [21,22,24].

The autophagic degradation of Ssn2/Med13 (outlined in Figure 1A) utilizes the core autophagic machinery but is independent of known nucleophagy mechanisms, known receptor proteins, and Atg11. In short, following nitrogen

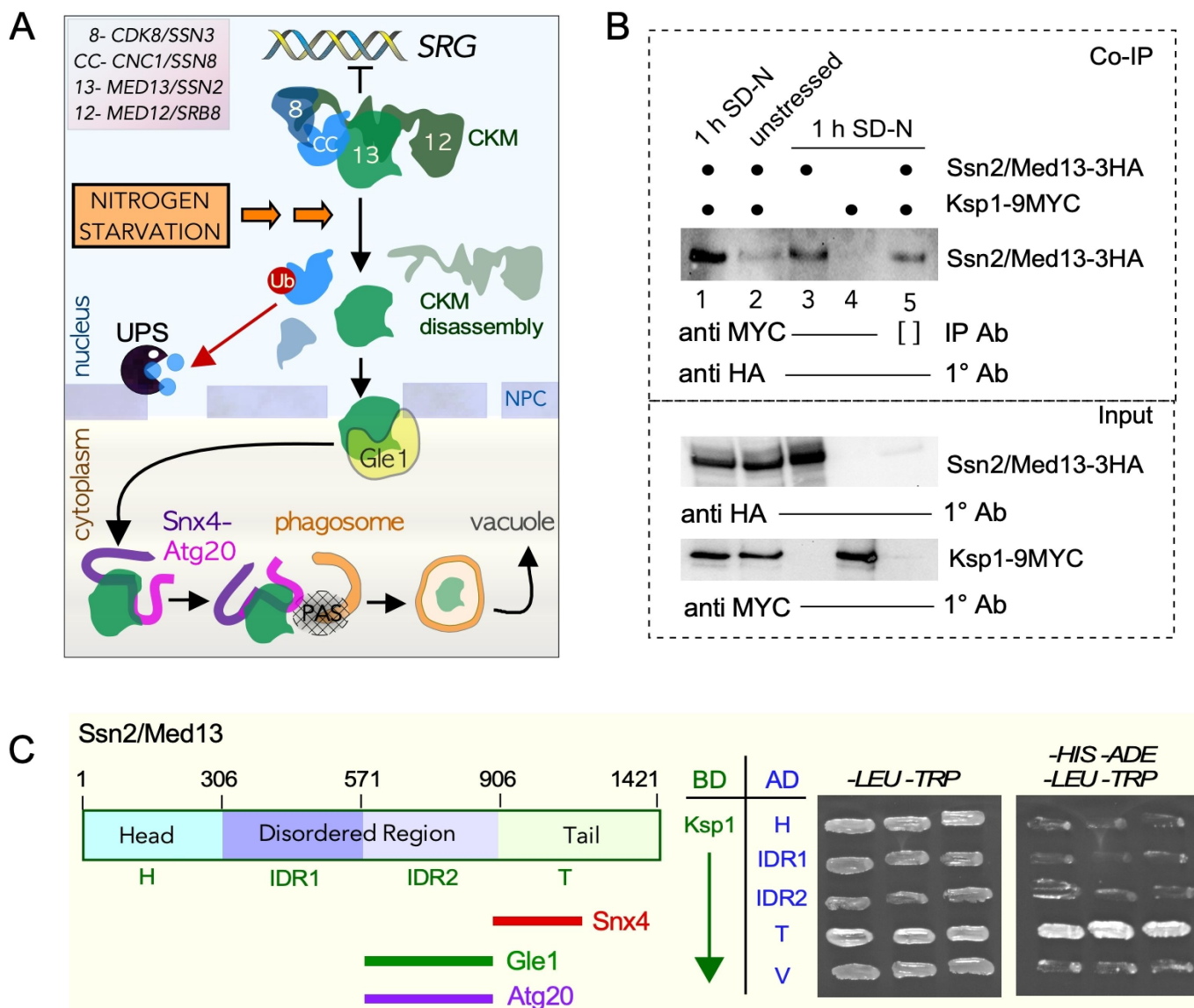


Figure 1. Ksp1 interacts with Ssn2/Med13. (A) Schematic of Snx4-assisted autophagy (SAA) of Ssn2/Med13 following nitrogen starvation. In replete media, the Cdk8 kinase module (CKM) of the mediator complex predominantly represses stress-responsive genes, including *ATG8*. Following nitrogen starvation, the CKM is disassembled, allowing the upregulation of these genes. Nitrogen starvation triggers Ssn8/cyclin C degradation by the UPS within the nucleus [22]. It also triggers the re-localization of Ssn2/Med13 to the cytosol, which requires the cytoplasmic nucleoporin Gle1. Once at the nuclear periphery, Ssn2/Med13 is transported to the autophagosome machinery by the Snx4-Atg20 sorting nexin heterodimer. Ssn2/Med13 is then sequestered into autophagosomes and degraded via autophagic degradation, and the sorting nexins are recycled back to the cytosol [21]. (B) Co-immunoprecipitation analysis of Ssn2/Med13-HA and Ksp1-9MYC before and after nitrogen starvation. Cells harboring Ssn2/Med13-3 HA and Ksp1-MYC (lanes 1, 2, & 5) or respective vector controls (lanes 3 & 34) were immunoprecipitated from whole cell lysates obtained from *pep4Δ prb1-Δ1* cells before and following 1 h of nitrogen starvation. □ represents a no antibody control (lane 4). For input controls, Ssn2/Med13 and Ksp1 were immunoprecipitated from lysates using the indicated antibodies. (C) Y2H analysis of Ssn2/Med13 and Ksp1. The left panel depicts the known structural regions of Ssn2/Med13 and previously identified interactors [21]. Y2H Gold cells expressing Gal4-BD-Ksp1 and the indicated Gal4-AD-Med13 subclones were plated onto medium selecting for plasmid maintenance (left panel, *-LEU -TRP*) or induction of the *ADE2* and *HIS3* reporter genes (right panel).

starvation, Ssn2/Med13 exits the nucleus through the nuclear pore complex (NPC) mediated by the cytoplasmic nucleoporin Gle1, a member of the RNA remodeling complex [25]. Ssn2/Med13 is retrieved from the nuclear periphery and degraded by Atg17-initiated phagophores anchored at the vacuole. Efficient transfer of Ssn2/Med13 to phagophores requires the sorting nexin heterodimer Snx4/Atg24-Atg20, which binds Atg17 [21,26,27].

To meet the criteria of selective autophagy, SAA-TF requires an autophagy receptor protein that exclusively tethers Ssn2/Med13 to the autophagic machinery through interactions with Atg8. Previously, using a yeast two-hybrid (Y2H) screen, Ksp1 was identified as one of 34 new putative autophagic receptor proteins in the budding yeast [16]. We also identified Ksp1 in a mass spectroscopy screen, looking for Ssn2/Med13 interactors after nitrogen starvation [21]. Together, this led us to test if Ksp1 is the autophagic receptor for SAA of Ssn2-Med13.

Ksp1 is a serine/threonine-protein kinase in the casein kinase II subfamily. This kinase was first identified as a high copy suppressor of a temperature-sensitive allele of *Srm1/Prp20*, a nucleotide exchange factor for Ran/GSP1 proteins [28]. Transcriptional profiling revealed that Ksp1 signaling affects various genes, including those required for pseudohyphal filamentation, amino acid biosynthesis, and metabolism [29–31]. How Ksp1 exerts this control remains unclear, but proteomic studies identified Ksp1 to be a component of cytoplasmic stress granules in response to glucose starvation [32,33]. In physiological conditions, Ksp1 contributes to negatively regulating autophagy. Here PKA-mediated phosphorylation of Ksp1 activates this kinase, which contributes to autophagy inhibition by activating the TORC1 pathway [34–38]. In support of this mechanism, *in vitro* studies have shown that PKA directly phosphorylates Ksp1 [30,39]. In contrast, dephosphorylation of Ksp1 at the same PKA sites hyper-activates Ksp1 in response to glucose starvation, which permits it to directly phosphorylate the translation initiation factor Tif4631/eIF4G1 [40]. Collectively, these studies demonstrate that Ksp1 has multifaceted regulatory roles that vary depending on the stress. Here, we define a kinase-independent role of Ksp1 that supports autophagy by serving a receptor protein for Ssn2/Med13 in Snx4-assisted autophagy.

Results

Ksp1 and Ssn2/Med13 interact following nitrogen starvation

To further define components of the SAA pathway, we used a mass spectroscopy screen to identify proteins that interact with Ssn2/Med13-HA following nitrogen starvation (SD-N) [21]. In this screen, we identified Ksp1 as a potential interactor. Co-immunoprecipitation analysis between Ssn2/Med13-HA and endogenous Ksp1-MYC both before (lane 2) and following 1 h (lane 1) in SD-N confirmed that the

interaction between these two proteins is significantly enhanced following nitrogen starvation (Figure 1B). This interaction was confirmed using yeast two-hybrid (Y2H) analysis. As full-length Ssn2/Med13 fused to the Gal4-activating domain represses transcription [21], we used a set of Ssn2/Med13 constructs that span the length of the protein (Figure 1C, left-hand panel [41]). The results show that the structured tail domain of Ssn2/Med13 interacts with Ksp1 (Figure 1C right-hand panel).

In SAA, Ssn2/Med13 translocates from the nucleus to growing phagophores for delivery to vacuoles [21]. Using fluorescence microscopy, we determined the subcellular localization of Ksp1-GFP and Ssn2/Med13-mNeonGreen (hereafter Ssn2/Med13-mNeon) following nitrogen starvation. First, we monitored endogenous Ksp1-GFP in cells harboring Nup-49-mCherry to mark the nucleus. As previously reported [40], Ksp1-GFP was predominantly located in the cytoplasm in SD media, although some nuclear staining was also observed upon quantification (Figure S1, upper panels). However, unlike filamentous growth [30], Ksp1 does not accumulate in the nucleus in SD-N (Figure S1, lower panels). Next, using endogenous Ksp1-mCherry and Ssn2/Med13-mNeon, we asked if Ssn2/Med13 colocalizes with Ksp1 as it transitions from the nucleus to the vacuole. These studies were performed in *pep4Δ prb1Δ.1*, a vacuolar protease mutant, in which autophagic bodies accumulate in the vacuolar lumen [42,43]. In unstressed cells, Ssn2/Med13-mNeon was nuclear [21], while Ksp1-mCherry was predominantly cytoplasmic [40]. Following nitrogen starvation, cytoplasmic Ksp1 foci appeared, which could also be captured colocalizing with cytoplasmic Ssn2/Med13 as it transitions from the nucleus to the vacuole (Figure 2A). These results agree with the co-IP studies, showing that Ksp1 and Ssn2/Med13 interaction occurs following starvation.

Ssn2/Med13 accumulates outside the vacuole in mutants defective in autophagic cargo delivery [21]. Specifically, in *atg8Δ* cells which are defective in phagophore expansion [44], we observed Ssn2/Med13 colocalizing with Atg2 and Atg7, two components of the phagophore [45,46]. In cells harboring a *vam3Δ* allele, a fusion deficient t-SNARE mutant [47–49], Ssn2/Med13 colocalizes with Atg8, which conjugates to phagophore membranes [17]. We also captured endogenous Ksp1-mCherry colocalizing with Ssn2/Med13-mNeon in *atg8Δ* and *vam3Δ* cells only following nitrogen starvation (Figure 2B,C respectively). This suggests that Ssn2/Med13 interacts with Ksp1 at the PAS before being delivered to vacuoles for proteolysis.

Ksp1, but not its kinase activity, is required for the autophagic degradation of Ssn2/Med13

We next addressed whether Ksp1 is required for the autophagic degradation of Ssn2/Med13. Quantitative western blot coupled with linear regression analysis of endogenous Ssn2/Med13-MYC revealed that the half-life of Ssn2/Med13 was >15 h in *ksp1Δ* compared to the 2.5 h half-life observed

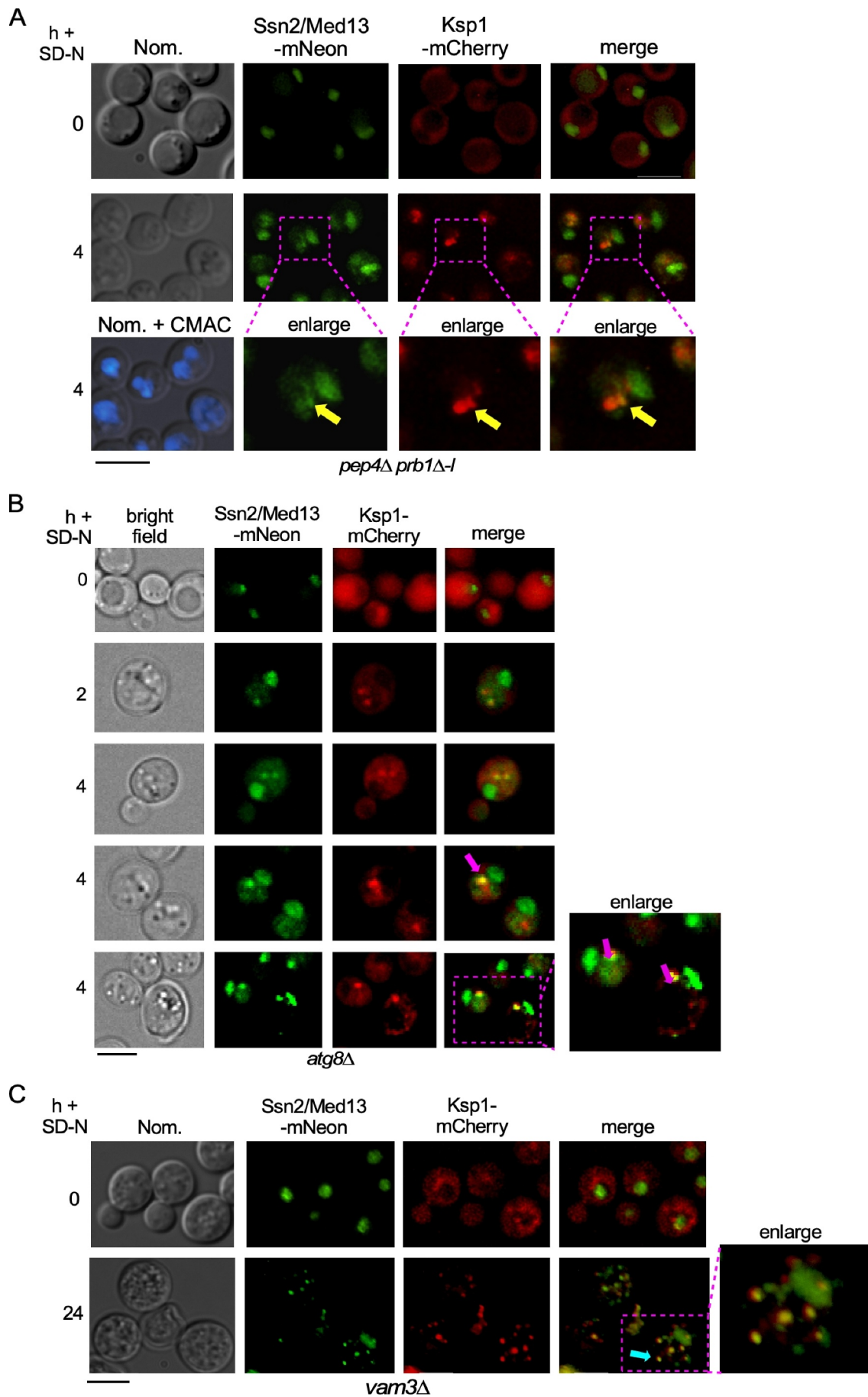


Figure 2. Ssn2/Med13 colocalizes with Ksp1 in the cytosol following nitrogen starvation. (A) Fluorescence microscopy of endogenous Ssn2/Med13-mNeongreen and

in wild-type cells Ksp1 (Figures 3A,B and S3A). These results show that the autophagic degradation of Ssn2/Med13 requires Ksp1. In contrast, the degradation of Ssn8/cyclin C, a CKM component destroyed by the UPS in nitrogen starvation [22], does not require Ksp1 (Figure S2A and S2B). This indicates that Ksp1 is only required for the degradation of autophagic substrates.

Ksp1 is a serine-threonine kinase that is activated by protein kinase A (PKA) in replete media at five consensus PKA sites (RRxS/T) [30,36–39]. This activation is required for Ksp1 to help suppress autophagy via the TORC1 pathway [35]. In contrast, we observed no differences in the decay rate of Ssn2/Med13 following nitrogen starvation in *ksp1Δ* cells harboring either wild-type Ksp1 or a kinase-dead mutant (*ksp1^{K47D}*) [28] (Figures 3C,D, respectively). These findings indicate that Ksp1 kinase activity is not required for Ssn2/Med13 degradation. They also revealed a second kinase-independent role for Ksp1 in autophagy. Its kinase-dependent role contributes to suppressing autophagy in physiological conditions [35], whereas its kinase-independent role mediates the autophagic degradation of Ssn2/Med13 and maybe other unknown substrates.

Ksp1 and Atg8 colocalize following nitrogen starvation

Ksp1 was previously identified in a Y2H screen as one of 38 new Atg8 interactors [16]. In this study, the authors propose that these Atg8 interactors represent novel autophagic receptors. As Ksp1 delivers Ssn2/Med13 to the vacuole, it could act as a cargo receptor for this CKM member. To test this, we asked if Ksp1 and Atg8 interact using fluorescence microscopy. In log-phase cells, growing SD media, very few GFP-Atg8 foci were observed, and Ksp1-mCherry was predominantly cytoplasmic (Figure S2C). Following two h in SD-N, most cells contained GFP-Atg8 foci that were observed colocalizing with Ksp1-mCherry (Figure 4A). Also, we captured this interaction only following nitrogen starvation in *vam3Δ* where Atg8 foci accumulate in mature autophagosomes (Figure 4B and S2C) [53]. Together these results indicate that Ksp1 and Atg8 colocalize at the PAS.

We next used Y2H analysis to confirm the colocalization studies and determine how Ksp1 interacts with its cargo and Atg8. To guide us on the design of Gal4-BD-Ksp1 constructs, we used structure prediction analysis of Ksp1 using IUPred3 [50–52]. This algorithm predicts the tendency of protein regions to have negligible folded tertiary structures, called intrinsically disordered regions (IDRs). The IUPred3 analysis results (Figure 4C, red line) revealed that only the amino terminus of Ksp1, which contains the conserved kinase domain, is structured. The remaining two-thirds of Ksp1 is highly unstructured, containing multiple IDRs. We next asked if regions within these IDRs contain molecular recognition features (MoRFs) that have the potential to transition to a structured conformation by interaction with a globular

protein partner [51,54]. This feature allows IDRs to interact with multiple binding partners and is observed in many proteins required for autophagy [55]. Moreover, it is significant as many Atg8 interacting motifs (AIMs) on receptor proteins lie within ANCHOR regions (see below) [56]. Analysis of Ksp1 using ANCHOR2 [57,58] revealed that its large IDR contains multiple potential MoRFs (Figure 4C, blue line). This analysis is consistent with the model that Ksp1 is an autophagic receptor protein, possibly of multiple cargos.

Based on this structural information, three Gal4-BD-Ksp1 constructs were generated, one spanning the kinase domain (KD), and two spanning the large unstructured region called disordered domain 1 (DD1) and 2 (DD2) (Figure 4C, bottom panel). Only the C-terminal construct (Gal4-BD-DD2, amino acids 681–1029) interacted with the Gal4-AD-Atg8 but not vector controls (Figure 4D). We also observed the interaction of Ksp1[DD2] with Ssn2/Med13 (Figure S4A). Together, these results are congruous with the model that Ksp1 is an autophagic receptor protein for this CKM member. As anticipated by this model, Y2H analysis revealed that Ssn2/Med13 and Gal4-BD-Atg8 do not interact [21]. To alleviate concern that DD2 interactions may be nonspecific due to its high IDR content, we showed that it does not interact by Y2H analysis with two other miscellaneous proteins (human cyclin C and yeast Ume6) fused to Gal4-AD (Figure S4B). In summary, these Y2H studies show that Ksp1 interacts with both Atg8 and Ssn2/Med13, supporting the model that Ksp1 is the receptor protein for Ssn2/Med13.

Ksp1 is degraded by autophagy following nitrogen starvation

A hallmark of receptor proteins is that they are engulfed in autophagosomes alongside their cargos [2]. Consistent with its putative receptor protein role, Ksp1 levels were reduced following nitrogen starvation with an apparent half-life of 2.6 h (Figure 5A, B, and S3B). Cycloheximide translation inhibition assays revealed that the half-life of Ksp1 was ~7 h in unstressed cells (Figure S4C), arguing that Ksp1 is actively degraded in SD-N. Moreover, upon repeating these assays in *pep4Δ* and *atg8Δ* strains, the decay rate of Ksp1 in SD-N was significantly slower with half-lives of over 15 h and 6.3 h, respectively (Figure 5A,B). The faster decay rate of Ksp1 observed in *atg8Δ* compared to *pep4Δ* suggests that if Ksp1 cannot reach the vacuole, it may be subjected to proteolysis by the UPS. However, Ksp1 was still degraded in *ump1Δ* cells that are defective in 26S proteasome assembly [59–62], and its decay rate in *ump1Δ atg1Δ* was not significantly different from *atg8Δ* (Figures 5C,D). Together, this indicates that following nitrogen depletion Ksp1 is subjected to autophagic degradation in the vacuole.

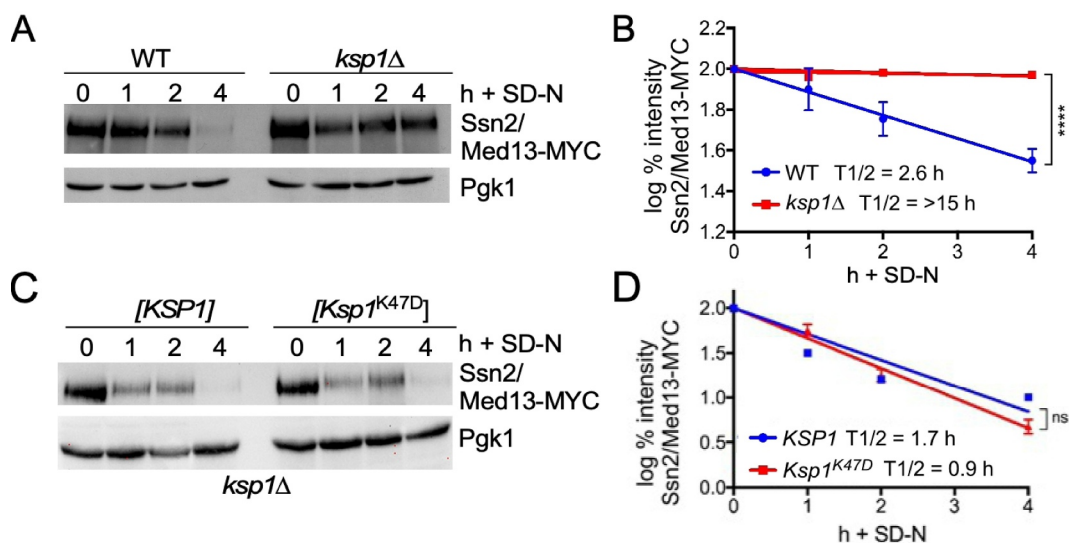


Figure 3. Ksp1 is required for the autophagic degradation of Ssn2/Med13. (A) Western blot analysis of extracts prepared from wild type or *ksp1Δ* expressing endogenous Ssn2/Med13-9MYC resuspended nitrogen starvation medium (SD-N) for the indicated times. (B) Linear regression analysis and half-life of Ssn2/Med13-MYC levels obtained in A. $N = 3$. **** $P \leq 0.0001$. (C) As in A, except in *ksp1Δ* cells harboring either Ksp1-GFP or a kinase-dead allele (K47D) expression plasmids were examined. (D) Linear regression analysis and half-life of Ssn2/Med13-9MYC protein levels obtained from C, $N = 3$. Pgk1 levels were used as loading controls.

To confirm these results, we tried to measure the autophagic flux of Ksp1-GFP by western blot analysis. This assay is based on the finding that GFP is protected from rapid degradation in the vacuole compared to its fusion partner [63–65]. Unfortunately, we were unable to visualize Ksp1-GFP by this method. However, using fluorescence microscopy, we observed Ksp1-GFP in the vacuole in a *pep4Δ* strain after 18 h in SD-N, whereas it remained predominantly cytoplasmic in *atg8Δ* cells (Figure 5E, quantified in S4A). Moreover, kinase-dead Ksp1^{K47D}-GFP, which is predominantly cytoplasmic in unstressed cells (Figure S4D), is also observed in the vacuole in *pep4Δ* cultures following SD-N treatment (Figure 5F), supporting the model that Ksp1 kinase activity is not required for its autophagic degradation.

Ksp1 interacts with the conserved receptor protein docking site on Atg8

Selective autophagy receptors interact with Atg8 through a conserved Atg8-family interacting motif (AIM), also known as LC3-interacting region (LIR) in more complex eukaryotes, that tightly fits into two conserved hydrophobic pockets on Atg8 known as the LIR/AIM docking site (LDS) [66,67]. The hydrophobic pockets are named the W and L-sites because they interact with tryptophan and leucine residues in AIMs, respectively [66–68]. To ask if Ksp1 requires a functional LDS for its autophagic degradation, we monitored its autophagic degradation in *atg8Δ*, harboring mutations in both sites (Y49A and L50A – named Atg8[LDS]). The results show that Atg8[LDS] significantly stabilized Ksp1 protein degradation in SD-N compared to the WT allele (Figure 6A), mirroring the half-life seen in *atg8Δ* (Figure 6B and S3C).

Similar to previous studies [68], we observed GFP-Atg8 [LDS] localization at the PAS after four h in nitrogen starvation and accumulation in vacuoles to be significantly

decreased in *atg8Δ* cells harboring GFP-Atg8[LDS] compared to GFP-Atg8 in SD-N (Figures 6C–E, S5A–C). Similarly, the vacuolar accumulation of Ksp1 in Atg8[LDS] was severely impaired (Figure 6C, quantified in 6F and S5B, S5C). These results agree with a previously published report in which *in vitro* dot blot binding assays were used to show that Ksp1 interacts with processed Atg8 (amino acids 1–116) [69], but not with the processed Atg8[LDS] mutant [16]. This is significant as the processing of Atg8 by removal of its C terminus by Atg4 is required for its recruitment to the PAS [70]. Together, these results support the model that Ksp1 directly interacts at the Atg8 docking site.

Ksp1 contains a canonical Atg8-family interacting motif

We next asked if Ksp1 contains a canonical AIM, originally described as ([W/F/Y]xx[L/I/V]) [67] but redefined to include two additional upstream amino acids (outlined in Figure S6A) [56,71,72]. Also, functional AIMs tend to depend on acidic residues surrounding the central core motifs and lie within a MoRF [56]. The iLIR database, which incorporates all these predictors into its logarithm, identified nine putative AIMs in Ksp1 (Figure S6B). The sole AIM found at the carboxy terminus of Ksp1 (NNWLIL_{1022–1025}, termed Ksp1[AIM1]) had the highest conservation of pattern alignment. Using computer modeling algorithms (ClusPro, Alpha fold) [73–76], this AIM fitted with high confidence into the hydrophobic LDS pocket of Atg8 (Figure 7A –one representative model and see Figure S6C for ribbon model). Computer modeling determined the potential ability of the various configurations of the mutated AIM1 (W1022A, L1025A, W1022A L1025A, and WLIL-AAAA) to fit into the hydrophobic pocket of Atg8. The results (Figure S6D) clearly show that, compared to the WT AIM, the mutants are significantly less able to fit into the pocket (orange scores). Instead, they lie either above (pink) or

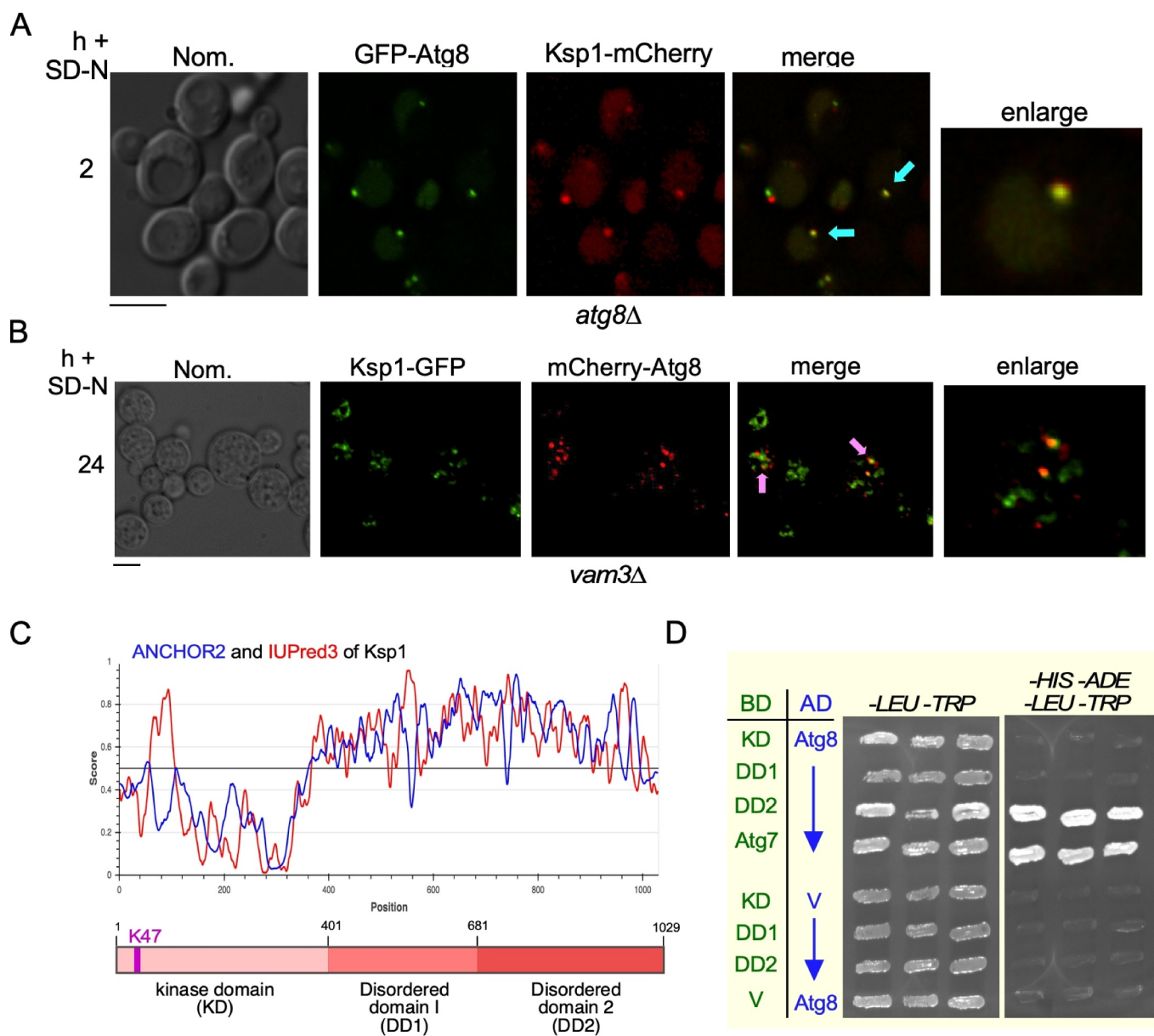


Figure 4. Ksp1 interacts with Atg8 following nitrogen starvation. (A) Fluorescence microscopy of endogenous Ksp1-mCherry in *atg8Δ* harboring GFP-Atg8 after 2 h nitrogen depletion. The blue arrow denotes the colocalization of Atg8 and Ksp1. (B) As in A, except the experiment was conducted in *vam3Δ* cells after 24 h in SD-N. The pink arrow denotes colocalization. Scale bar: 5 μ m. (C) IUPred3-long [50–52] (red) analysis of Ksp1. The score corresponds to the probability of the given residue being part of a disordered region (IUPred3-long). Residues with a predicted score above and below 0.5 are considered disordered and ordered, respectively. Overlaid in blue is the ANCHOR2 plot, which assesses the probability of disordered binding regions transitioning between structured and unstructured states. A schematic of full-length Ksp1 divided into the three domains used in Y2H analysis is shown underneath the profile. (D) Y2H Gold cells harboring the indicated Gal4-BD-Ksp1 subclones and Gal4-AD-Atg8. Gal4-BD-Atg8 and Gal4-AD-Atg7 were used as a positive control. V = vector. The cells were plated on media selecting for plasmid maintenance (left panel, -LEU -TRP) or expression of the *ADE2* and *HIS3* reporter genes (right panel).

below (cyan) this interface, indicating that Ksp1^{AIM1} is a strong candidate to be a functional AIM.

Previous studies have shown that other receptor proteins harboring changes in the conserved Atg8 interaction residues fail to interact with Atg8 using Y2H [66,67,77]. Consistent with this, mutation of W1022 and L1025 to alanine residues in Ksp1[DD2] (DD2^{W1022A,L1025A}) negatively affected, but did not completely eliminate, the Y2H Ksp1-Atg8 interaction (Figure 7B). In addition, deletion of this AIM (called *ksp1* [AIM1]) did not have a noticeable effect on Ksp1 degradation (Figures 7C,D), and Ssn2/Med13 was observed in the

vacuole following SD-N (Figures S6E and F). As no other Ksp1 domains interacted with Atg8 (see Figure 4) and Ksp1 [DD2] contains no other canonical aims (Figure S6D), this suggests that Ksp1[DD2] contains non-canonical AIM motifs that do not fit the iLIR sequence requirements. These motifs are hard to define as their Atg8 binding modes are case-specific and can depend upon different structural determinants [78]. They have been observed for Atg19, a receptor protein for the cytoplasm-to-vacuole targeting (Cvt) pathway [79–81], and the interaction of Atg8 with Hfl1 [82]. They have also been observed in mammalian receptor proteins [78].

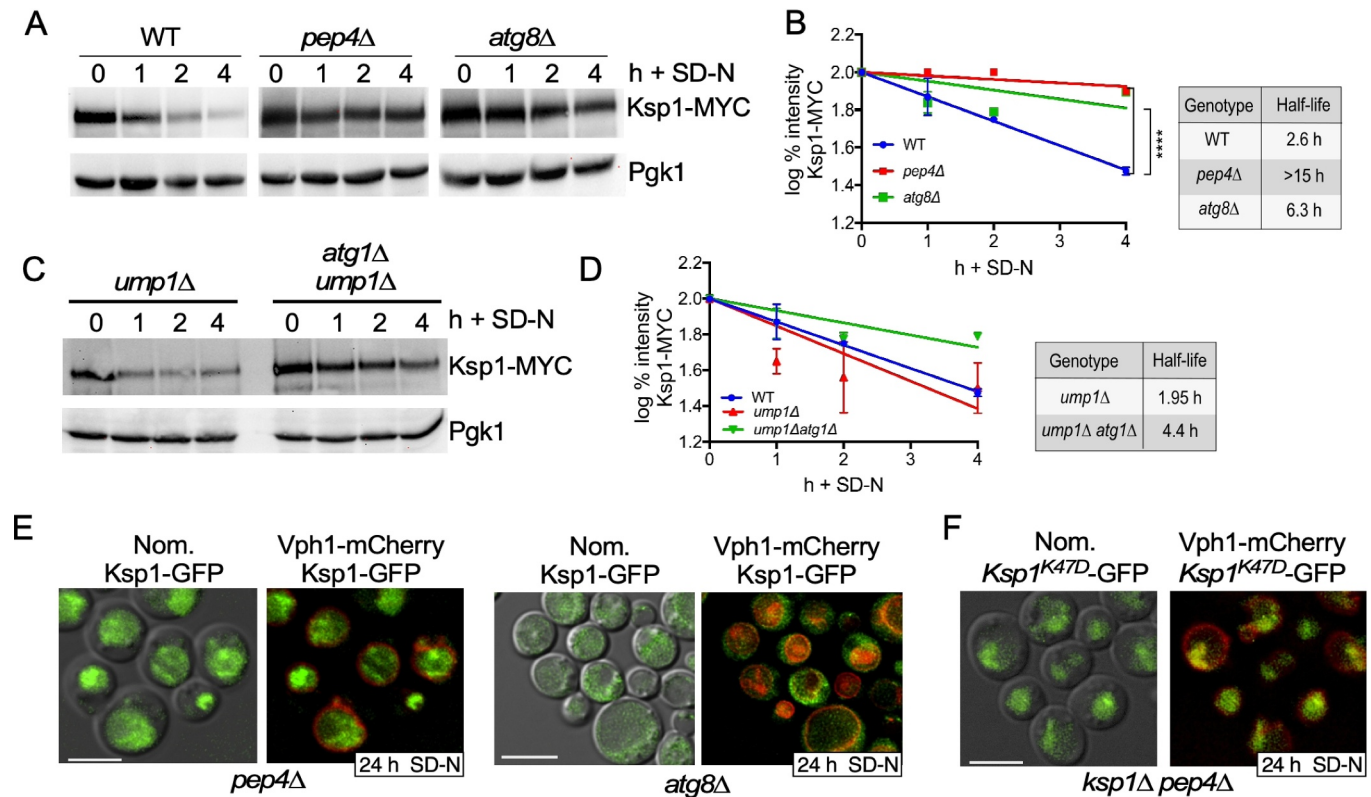


Figure 5. Ksp1 is an autophagic substrate. (A) Western blot analysis of protein extracts from endogenous Ksp1-9MYC following nitrogen starvation in the genotypes indicated. (B) Linear regression analysis of Ksp1-9MYC signals obtained in A. Pgk1 protein levels were used as the loading control. $N = 3$. $****P \leq 0.0001$. (C) Same in A, except experiments were performed in the indicated genotypes. (D) quantification of C. Ksp1-9MYC degradation kinetics in WT cells (blue line) was obtained from 5B and used as a comparison in 5D. (E) Fluorescence microscopy of endogenous Ksp1-GFP in either *pep4Δ* or *atg8Δ* cells following nitrogen starvation. Vph1-mCherry was used to mark the vacuoles. (F) As in E, except *ksp1Δ pep4Δ* harboring *ksp1^{K47D}*-GFP was monitored. Scale bar: 5 μ m.

An alternative explanation for SAA-Med13 not being affected in *ksp1[AIMΔ1]* cells is that an additional region of Ksp1 that was not detected by Y2H assays (see Figure 4) can bind to Atg8. To test this, we monitored the degradation kinetics of *ksp1[AIMΔ1]* coupled with another potential AIM mutant. We chose DLYEAI_{169–172} (*ksp1[AIM2]*), which lies within the structured amino-terminal domain of Ksp1 and had the second-highest PSSM score. In addition, FNFNNV_{405–410} (*ksp1[AIM3]*), which lies in Ksp1[DD1] (Figure S8A), was analyzed. We created *ksp1[AIM1Δ]^{Y169A, I172A}* and *ksp1[AIMΔ1,3]*. However, neither mutation stabilized Ksp1 following SD-N nor prevented Med13 from reaching the vacuole (Figures 7F and S8). These results favor the possibility that Ksp1[DD2] contains at least one non-canonical AIM.

The Atg17-Atg31-Atg29 complex interacts with Ksp1

In yeast, the PAS is initiated during selective autophagy by forming cargo-receptor complexes, which are recruited to the vacuole by Atg11. This provides a local clustering platform for Atg13 recruited Atg1, leading to trans-autophosphorylation and activation of Atg1 [83–85]. In contrast, bulk autophagy is initiated by forming a supramolecular structure of Atg13 and Atg1 with the trimeric Atg17-Atg31-Atg29 complex (17C) [86,87]. Similar to the selective degradation of Cue5 cargos (ubiquitinated aggregated proteins and dysfunctional

proteasomes [19,20]), the autophagic degradation of Ssn2/Med13 requires the 17C scaffold [21]. Therefore, using Y2H analysis, we asked if Ksp1 interacts with a member of the trimeric scaffold. As reported by others, Y2H analysis revealed that none of the trimeric scaffold complex members interacted with Atg8 [88] (Figure S9A). However, the carboxy terminus of Ksp1 interacted with both Atg29 and Atg31 (Figure S9B and S9C). Using 3-aminotriazole (3-AT) in Y2H analysis allows for differing levels of stringency when histidine-based growth selection is used, as it competitively inhibits the *HIS3* gene product [89]. Adding 50 mM 3-AT still permitted the Ksp1 interaction with Atg29 but not Atg31 (Figure 8A, upper panels). These results suggest that Ksp1 interacts with 17C. Previous studies have shown that mutation of the AIM in receptor proteins does not affect their interaction with scaffold proteins [77,90]. Likewise, the C-terminal Ksp1 Y2H construct harboring the L1025A mutation still interacted with Atg29 using Y2H analysis (Figure 8A, lower panels). Together, these results support the model that Ksp1 interacts with both Atg8 and the scaffold complex, with only the Ksp1-Atg8 interaction being dependent on an AIM.

The Atg17-Atg31-Atg29 scaffold complex recruits Ksp1 to the PAS

We next confirmed the Ksp1-Atg29 Y2H interaction using colocalization studies of live cells. Congruous with the Y2H

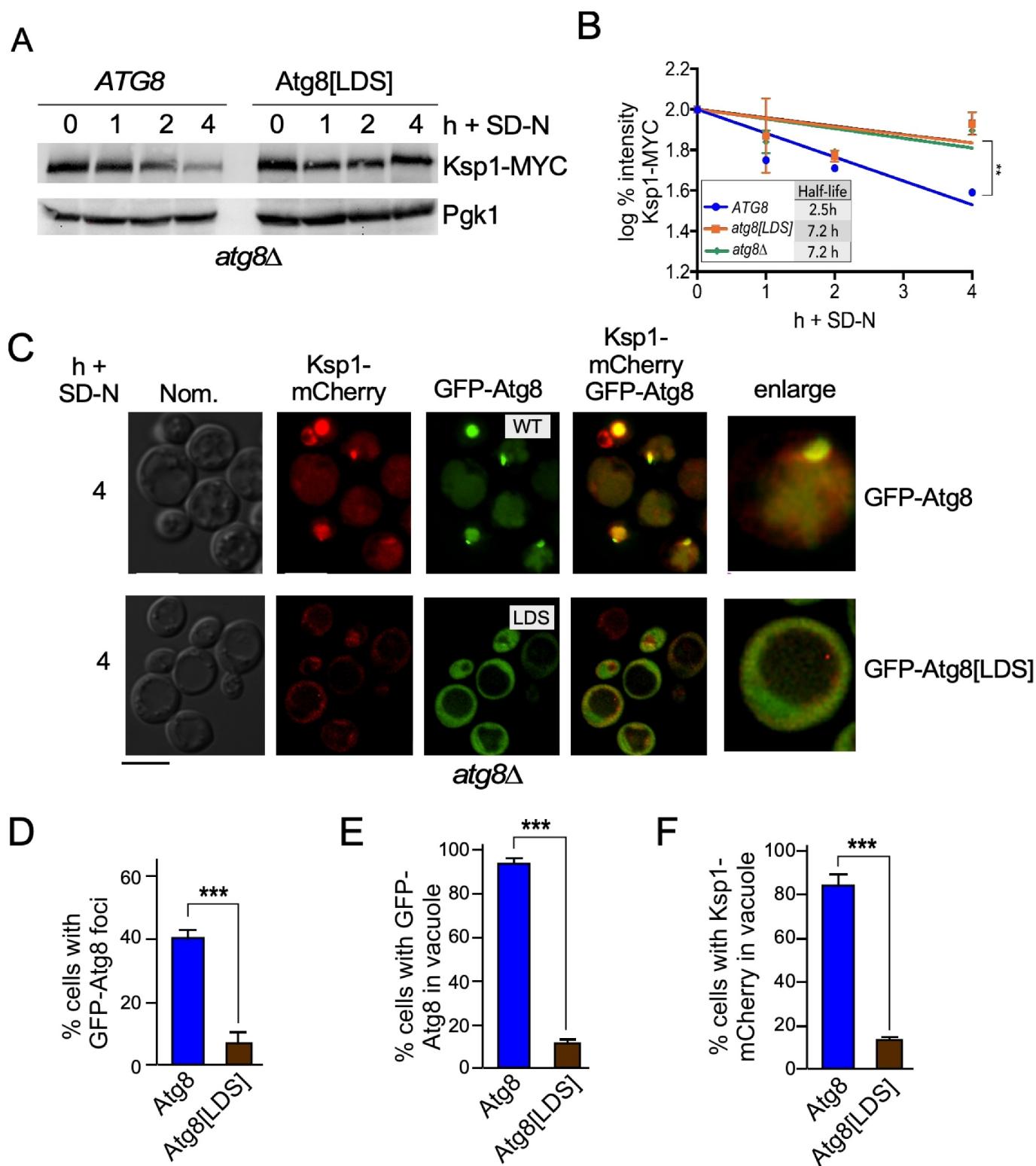


Figure 6. The autophagic degradation of Ksp1 requires the LDS motif of Atg8. (A) Western blot analysis of endogenous Ksp1-9MYC in *atg8Δ* cells expressing either WT or LDS alleles of GFP-Atg8 following nitrogen starvation. Pgk1 protein levels were used as the protein loading control. (B) Linear regression analysis and half-life of Ksp1-9MYC protein levels in the genotypes indicated. $N = 3$. $^{***}P \leq 0.005$. Ksp1-9MYC degradation kinetics in *atg8Δ* cells (blue line) obtained from Figure 5B was used as a comparison in panel B. (C) Fluorescence microscopy of endogenous Ksp1-mCherry in *atg8Δ* cells harboring plasmids expressing either the WT or *LDSΔ* allele of GFP-Atg8. (D) Quantification of foci GFP-Atg8 and GFP-Atg8[LDS] foci observed in *atg8Δ* after 4 h in SD-N. $N = 3$ (E) Quantification of cells observed with GFP-Atg8 or GFP-Atg8[LDS] in the vacuole in *atg8Δ* mutants after 4 h in SD-N. $N = 3$ (F) Quantification of cells observed with Ksp1-mCherry in the vacuole after 4 h in SD-N in *atg8Δ* harboring either GFP-Atg8 or GFP-Atg8[LDS]. $N = 3$.

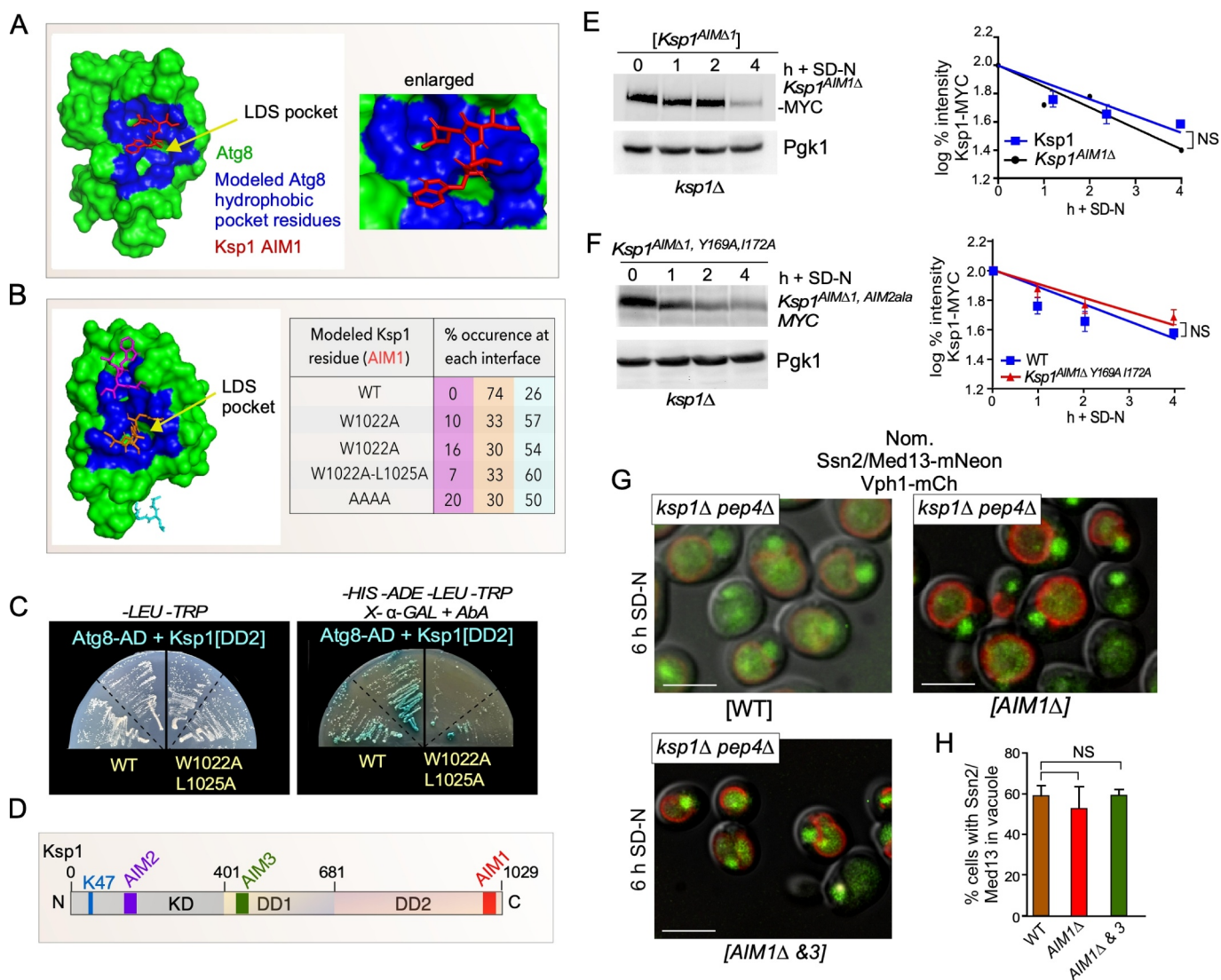


Figure 7. Ksp1 contains a single C terminal canonical AIM (A) Left panel: a representative image from computer modeling of Ksp1[AIM1] with Atg8 showing that it can associate with the hydrophobic LDS pocket (yellow arrow). The green denotes Atg8, the red Ksp1[AIM1], and the blue correlates with the hydrophobic pocket (LDS) of Atg8 (see material and methods for details). The right panel has an enlarged image demonstrating that the AIM1 residues engage with the LDS pocket. (B) Left panel. Representative image showing the interfaces on the hydrophobic pocket of Atg8 where wild type and mutant Ksp1 AIM could lie. Right panel: the % occurrence of the mutation shown in Ksp1[AIM1] was modeled onto the hydrophobic pocket region of Atg8. The orange position is the interacting region favored by WT AIM, whereas the pink and cyan positions that lie above and below the pocket are predominantly favored by the mutant alleles. (C) Y2H analysis of Gal4-BD constructs shown with Gal4-AD-Atg8. Two biological replicates were plated on medium selecting for plasmid maintenance (-LEU, -TRP, left) or interaction by induction of all four reporter genes, ADE2, HIS3, MEL1, and AUR1-C (right). (D) Schematic of Ksp1 showing the position of potential AIMs. (E and F) Quantitative western blot and linear regression analysis of *ksp1Δ* harboring the plasmids shown (square brackets) following SD-N. *ksp1Δ*[AIM1Δ, AIM2ala] represents the Ksp1 allele in which AIM1Δ was coupled with the Y169A and I172A mutations. Pgk1 protein levels were used as the protein loading control. $N = 3$ $**P \leq 0.005$. WT Ksp1 was obtained from Figure 5B and used as a comparison. (G) Fluorescence microscopy of *ksp1Δ pep4Δ* Ssn2/Med13-mNeon cells harboring the indicated plasmid following 6 h in SD-N. Scale bar: 5 μ m. (H). Quantification of G, counting the number of cells in which vacuolar Ssn2/Med13 was detected. $N = 3$.

results, we observed that endogenous Ksp1-mCherry colocalized with Atg29-GFP foci only following two h in SD-N (Figure 8B). In the hierarchy of autophagy proteins loading onto the PAS, 17C arrives at the PAS found at perivacuolar sites before Atg8 [87,91]. Therefore, using fluorescence microscopy, we asked if Ksp1-mCherry could interact with the PAS (marked by Atg29-GFP) in the absence of Atg8. The results showed that Ksp1 colocalized with Atg29-GFP in *atg8Δ* cells after 2 h in SD-N (Figure 8B). These studies strongly support a model in which, after autophagy initiation, Ksp1 is anchored at the perivacuolar PAS by Atg29. They also define Ksp1 as an autophagic receptor protein that works with expanding phagophores most associated with nonselective autophagy.

However, instead of packaging indiscriminate parts of the cytoplasm, we show that these phagophores also recruit targeted cargo.

Snx4 is not required for the recruitment of Ksp1 to the PAS

The sorting nexin heterodimer Snx4-Atg20 assists cargo degradation in many selective pathways, including mitophagy, pexophagy, and ribophagy [26,92–95]. In addition, the recruitment of a subset of transcriptional regulators, including Ssn2/Med13, to phagophores is aided by this heterodimer [26]. In this model, Ssn2/Med13 directly binds to Snx4-

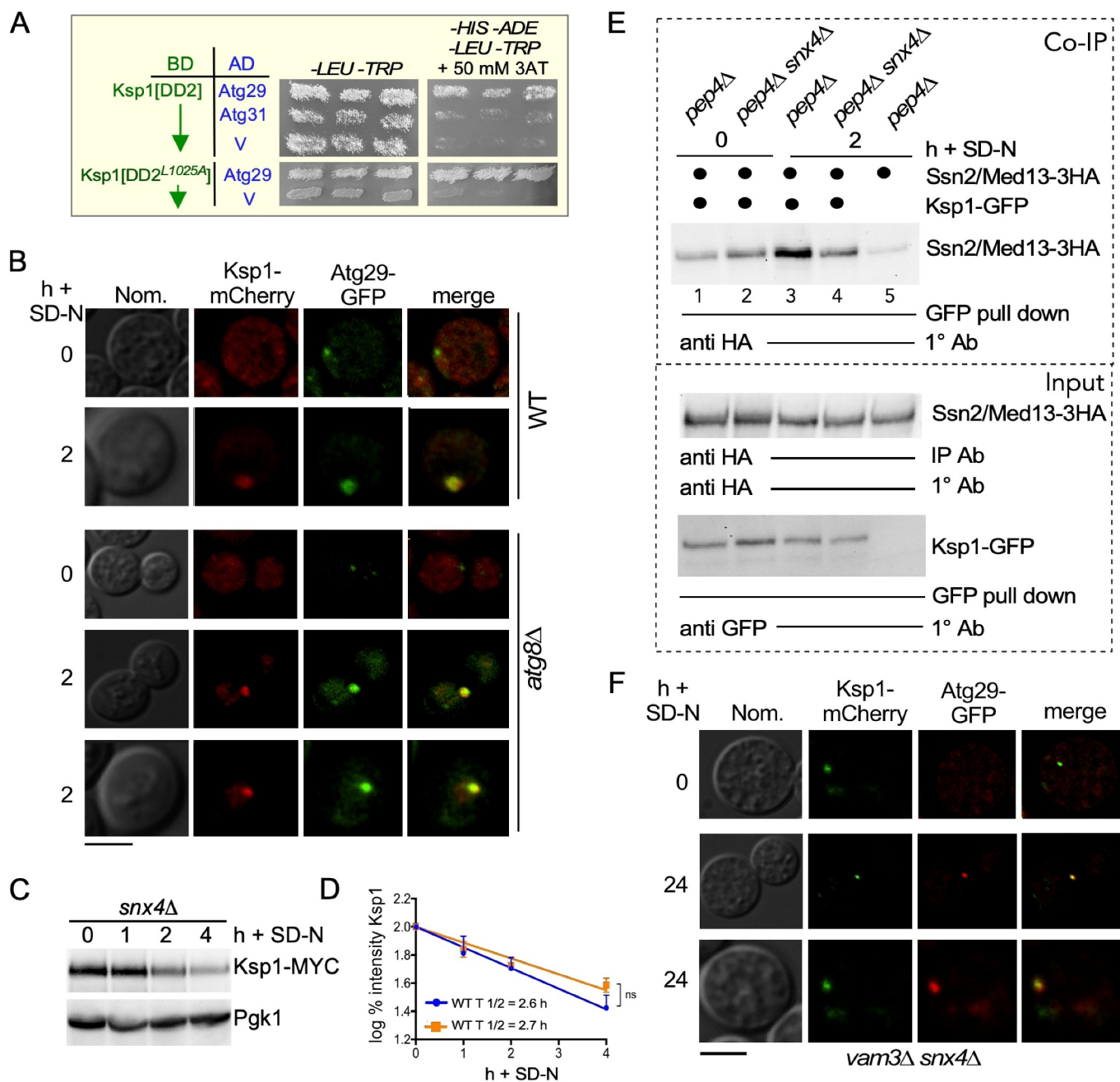


Figure 8. The Atg17 complex recruits Ksp1 to phagophores independent of Snx4. (A) Y2H analysis. Upper panels; Gal4-BD-Ksp1[DD2] with either Gal4-AD-Atg29, Gal4-AD-Atg31, or a vector control. Lower panels; Gal4-BD-Ksp1[DD2]^{L1025A} with either Gal4-AD-Atg29 or a vector control. Cells were streaked on medium, selecting for plasmid maintenance (left) or induction of reporter genes (right) by Y2H interaction. To increase the stringency of *HIS3* induction, 50 mM 3-aminotriazole was added to the media. (B) Single-plane fluorescence microscopy images of Ksp1-mCherry and Atg29-GFP before and after nitrogen starvation in wild-type and *atg8Δ* cells. Bar: 5 μ m. (C) Western blot analysis of Ksp1-9MYC following nitrogen starvation in *snx4Δ*. (D) Quantification of B. Ksp1-9MYC degradation kinetics in WT cells (blue line) was derived from Figure 5A. (E) GFP affinity-isolation analysis of Ksp1-GFP and Ssn2/Med13-3HA in the presence and absence of Snx4. Protein extracts made from the mutants indicated before and after 2 h SD-N were collected on “chromotek GFP agarose beads,” washed and separated by SDS-PAGE. The membrane was initially probed with the anti-HA (co-IP), then stripped and reprobed with anti-GFP for input control. For the Ssn2/Med13 input control Ssn2/Med13-3 HA was immunoprecipitated from lysates using the indicated anti-HA as described in Figure 1B. (F) Single plane fluorescence microscopy images of Ksp1-mCherry and Atg29-GFP before and following nitrogen starvation in *vam3Δ snx4Δ* cells. Bar: 5 μ m.

Atg20, and the complex is recruited to the PAS by Snx4-Atg17 interaction [26]. Consistent with this, in the absence of Snx4, co-IP analysis revealed that the interaction between Atg17 and Ssn2/Med13 is diminished [21]. To ask if Snx4-Atg20 also recruits Ksp1 to the PAS, we monitored the autophagic degradation of endogenous Ksp1 in *snx4Δ*. The results (Figures 8C and quantified in 8D) show that Ksp1 is still degraded following nitrogen starvation, indicating that Snx4 is not required to

deliver Ksp1 to the PAS. Supporting this, Ksp1-GFP affinity isolation of Ssn2/Med13-3 HA were significantly enhanced following nitrogen starvation in *pep4Δ* but not in *pep4Δ snx4Δ* (Figure 8E). Also, Atg29-GFP foci colocalized with Ksp1-mCherry in *vam3Δ snx4Δ* cells following nitrogen starvation (Figure 9F). These results support the model that Snx4-Atg20 delivers cytoplasmic Ssn2/Med13 to growing autophagosomes but is not required to recruit Ksp1 to the PAS.

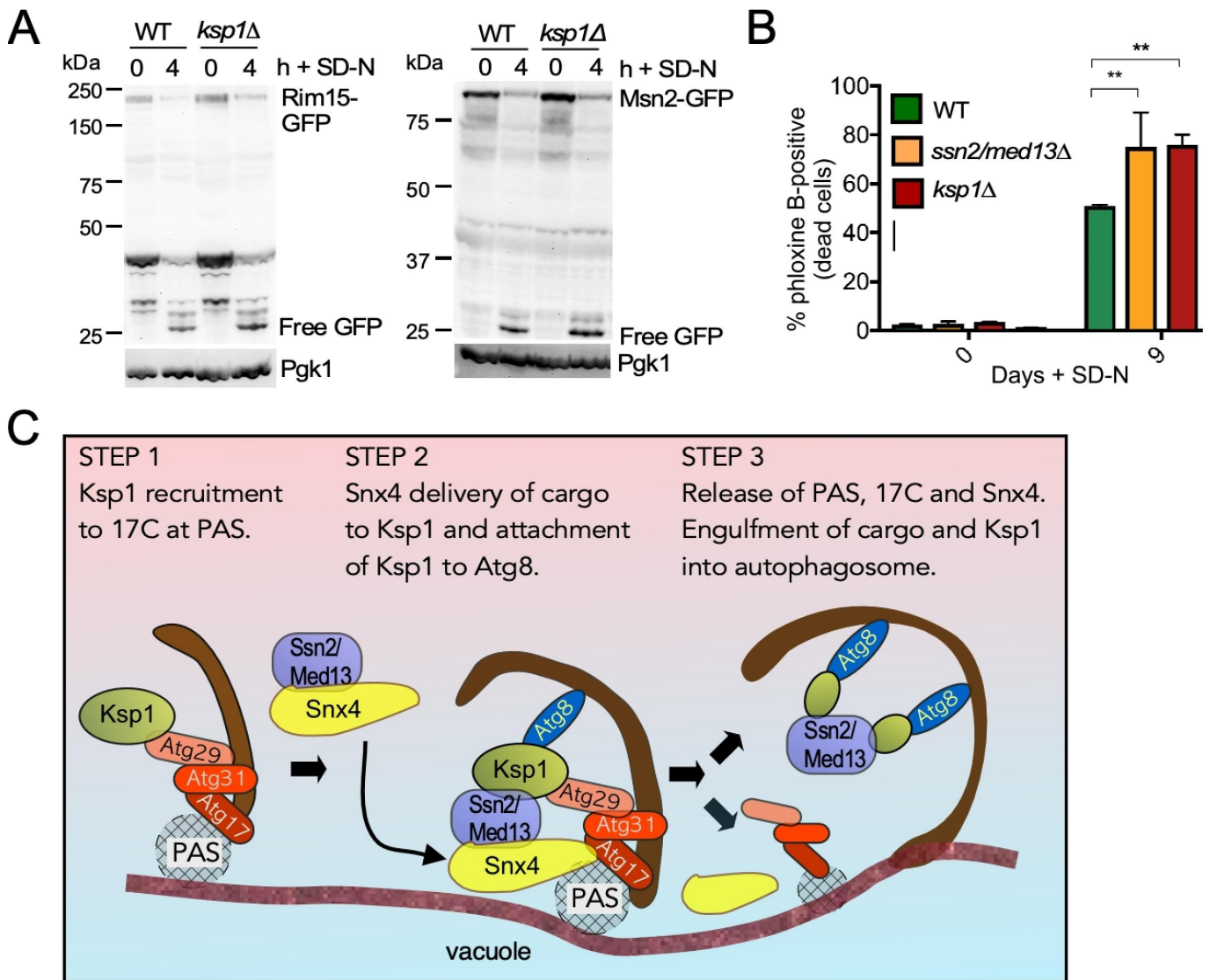


Figure 9. Ksp1 is required for survival, but this is not dependent upon the autophagic degradation of Rim15 and Msn2. (A) Autophagic cleavage assays of Rim15-GFP and Msn2-GFP in WT and *ksp1Δ* cells. For all assays, endogenous Pgk1 was used as a loading control. (B) Survival assays of the strains shown before and after 9 days in SD-N. (C) Schematic of the receptor protein role of Ksp1 in the autophagic degradation of Ssn2/Med13. Experimentally determined protein interactions are shown. Ksp1 is recruited to perivacuolar phagophore assembly sites (PAS) by Atg29 of the trimeric scaffold complex. Ssn2/Med13 is recruited to the PAS by Snx4-Atg20. It remains unknown whether Ssn2/Med13 can bind to the trimeric complex. Thereafter the trimeric complex, PAS factors, and Snx4-Atg20 are released from autophagosomes [8,21], whereas the interaction of Ksp1 with the LDS region of at least two Atg8 sites, delivers its cargo, Ssn2/Med13, to autophagosomes for eventual degradation in the vacuole.

Ksp1 is not an autophagic receptor for Rim15 or Msn2

Rim15 and Msn2 are also SAA cargos [21]. We, therefore, asked whether these transcription factors also use Ksp1 as an autophagic receptor. However, using autophagic GFP cleavage assays, we observed free GFP cleaved from Rim15-GFP and Msn2-GFP following nitrogen starvation in both wild-type and *ksp1Δ* cells (Figure 9A). This suggests that the autophagic degradation of these transcriptional activators may be mediated by an unknown receptor protein, possibly by one of the 34 putative Atg8 interactors previously identified [16]. These results also suggest that Snx4 transports selective substrates, including transcription factors, RNA, ribosomes, and proteasomes, to the autophagic machinery [21,27], and Ksp1 functions as a receptor protein at the PAS for only a subset of these proteins. This role may be necessary for survival, as *ksp1Δ* or *ssn2/*

med13Δ mutants were less able to survive nine days of nitrogen depletion compared to wild type (Figure 9B).

Discussion

In its infancy, the field of autophagy depicted the lysosome as a major nonselective dumpsite within the cell. Since then, the pool of autophagic substrates has expanded from excess or damaged organelles and protein aggregates to fully functional multi-subunit complexes and single proteins. In the last decade, a strong focus has been on discovering autophagic receptor proteins, which provide substrate specificity, acting as decision-makers in autophagy pathways [2,13,96]. Here we show that Ksp1 is the receptor protein for the autophagic degradation of a transcriptional regulator, Ssn2/Med13 (summarized in Figure 9C). This role is independent of its kinase

activity, demonstrating the dual functionality of this kinase. Data presented in this current study suggests a model in which Ksp1 is first recruited to the PAS, binding to 17C and Atg8. Next, Snx4-Atg20 delivers Ssn2/Med13 to PAS-bound Ksp1. Last, PAS factors and Snx4-Atg20 are removed from growing phagophores [8,21], and Ssn2/Med13 and Ksp1 are engulfed within autophagosomes. This finding supports the model that the autophagic degradation Ssn2/Med13 is highly discriminating. Firstly, Ssn2/Med13 is not only selectively targeted from among other transcription factors associated with chromatin, but also from within components of the CKM itself [21,24]. Secondly, the cytoplasmic Ssn2/Med13 engulfment by autophagosomes is not random but assisted by Snx4-Atg20, with Ksp1 acting as a receptor protein. Outlining its importance, the degradation of either Ssn2/Med13 and/or other Ksp1 cargos by this mechanism contributes to the survival of *S. cerevisiae* following nitrogen starvation.

Cargo receptors are characterized by their ability to bind cargo and facilitate the recruitment of autophagic machinery through the binding of Atg8 and a scaffolding subunit of the Atg1 complex. Thereafter cargo receptors are captured within autophagosomes, being finally degraded by vacuolar proteolysis alongside their cargos [2,96]. Here we report that Ksp1 fulfills these functions. Ksp1 specifically binds to Ssn2/Med13 and is required for its autophagic degradation (Figures 1–3). Ksp1 itself is also degraded by vacuolar proteolysis (Figure 5). Like other receptor proteins, Ksp1 directly binds to Atg8 (Figure 4), and this binding is dependent upon the conserved hydrophobic LDS pocket in Atg8 (Figure 6) and Atg8 interaction motifs in Ksp1. (Figure 7). These observations define Ksp1 as an autophagic receptor protein for Ssn2/Med13. Intriguingly, Rim15 and Msn2, other known cargos of SAA, do not require Ksp1 for autophagic degradation (Figure 9A). This suggests that other, unknown receptor proteins, could fulfill this role.

The interaction of Ksp1 with Atg8 is complex. Deleting the LDS region in Atg8 prevented the autophagic degradation of Ksp1 (Figure 6). Y2H revealed that only the C terminal domain of Ksp1 (Ksp1[DD2]) interacted with Atg8, but deletion of the single canonical AIM in Ksp1 [DD2] in full-length Ksp1 did not affect Med13 vacuolar proteolysis. Coupling this mutation with the deletion of two other potential AIMS also did not prevent SAA-Med13 in SD-N. The most likely interpretation of these results is that Ksp1^{DD2} contains one or more non-canonical AIMS. These motifs, also called non-canonical LIR motifs (CLIRs), are very case specific, making them hard to define by sequence analysis alone (reviewed in [78]). For example, the interaction between Atg19, a receptor protein for the Cvt pathway [79–81] is mediated by a canonical and two non-canonical AIMS (LxxL, FxxF) [79–81]. Other cases described CLIRs that possess a helical conformation and do not form an intermolecular beta-sheet with Atg8, a common feature of canonical AIMS. Other reported configurations include CLIRs with additional residues (FxxxxxxxxY, WxxxI) [82] as well as more simple motifs, including LVV [97]. Further experimentation is needed to define the potential CLIRs in Ksp1.

One potential advantage of possessing multiple AIMS is that it enables receptors to interact with multiple Atg8 proteins simultaneously, allowing its cargos to be exclusively captured within autophagosomes [81]. We recently have identified other Ksp1 cargos but do not know if they are engulfed alone, together, and/or with nonspecific cytoplasmic components. Furthermore, the induction of selective autophagy in mammalian cells also leads to bulk degradation of a portion of the cytosol. This mechanism, coined “bystander autophagy”, results in autophagosomes enriched for both specific and nonspecific cargos [98,99]. Thus, it’s possible that autophagosomes enriched for Ksp1 cargos could also capture nonspecific cytoplasmic material as well.

Cargo receptors in yeast also most commonly interact with the Atg11 scaffold protein leading to the nucleation of phagophores in the direct vicinity of cargo [90,92,100–105]. Thereafter cargo filled autophagosomes are delivered to the vacuole for degradation. The exception is Cue5, which, similar to Ssn2/Med13, does not require Atg11 but uses the trimeric Atg17 scaffold complex to deliver its cargos to expanding phagophores [19,20]. This is interesting as this scaffold nucleates phagophores which most commonly sequester random portions of cytoplasmic material during nitrogen starvation [106]. We now show that Ksp1 binds to Atg29 and colocalizes with this complex after nitrogen starvation at the PAS (Figure 8). Together, these results suggest phagophores nucleated by either scaffold utilize receptor proteins to sequester specific cargo. Alternatively, as the second job of 17C is to mediate efficient autophagosome-vacuole fusion [107], our results could mean that Ssn2/Med13 requires this second function of the trimeric scaffold. However, we favor the first explanation as this model best fits our results. Intriguingly, the separation of jobs for Atg11 and the trimeric scaffold complex is not so clear-cut in more complex eukaryotes [105]. For example, in mammalian cells, the Atg17 homolog, RB1CC1/FIP200 (RB1 inducible coiled-coil 1), combines the functions of both these yeast scaffold proteins, playing a role in selective and nonselective autophagy [108,109].

Currently, we do not know why Ssn2/Med13 is destroyed by SAA following nitrogen starvation, when it is destroyed by the UPS in the nucleus following ROS stress [41,110]. Like Ssn8/cyclin C, Ssn2/Med13 could have two cellular roles (a. k. a. day and night job). Its “day job” is transcriptional control of stress response genes [24]. Its starvation stress-induced night job occurs in the cytoplasm, before it is destroyed by SAA. One possibility is that Ssn2/Med13 could be RNA binding protein (RBP), as recent structural studies have identified an AGO (argonaute RISC component)-like bi-lobal architecture [111]. Characteristic of AGO proteins, Med13 contains four globular domains (N, PAZ, MID, and PIWI) and an L2 linker domain (L2-N) that may bind RNA, including non-coding RNAs. In higher eukaryotes, Ago-like proteins associate with micro-RNA (miRNA) to produce the miRNA silencing complex [112,113]. Moreover, AGO proteins, miRNAs, and their targets also can localize to processing bodies [114]. As *S. cerevisiae* does not contain other RNAi genes, the L2-N domain in Med13 could mimic an AGO-bound guide RNA [115]. However, in these studies, no density corresponding to

DNA or RNA was found within the L2 domain [111]. This has led to the hypothesis that post-translational modifications of L2-N may allow RNA binding. Further studies are needed to explore this hypothesis, but the current models underline that both transcriptional and post-transcriptional gene regulation are unappreciated functions of autophagy.

To conclude, the results presented here support the model that Ksp1 defines a new type of autophagic receptor protein. This role is independent of its kinase function, showing that Ksp1 has dual and opposing roles in regulating autophagy pathways. These findings broaden our knowledge of autophagy mechanisms and suggest that paradigms that define selective and nonselective autophagy pathways are merging. In support of this, it was recently revealed that specific RNA species tightly coupled with translation are degraded by autophagy in response to stress [116]. Like SAA of transcription factors, Snx4-Atg20 assists in autophagy-mediated mRNA degradation, suggesting that the pathways may have other unknown similarities [116].

Materials and methods

Yeast strains and plasmids

Experiments were primarily performed with endogenously labeled proteins in the *S. cerevisiae* W303 background [117] and are listed in Table S1. All strains were constructed using replacement methodology and details are available upon request [118]. The Y2H assays were performed in the Y2H Gold strain in which there are four integrated reporter genes (*ADE2*, *HIS3*, *MEL1*, and *AURE1-1*) (Takara 630,489, PT4084-1; Matchmaker Gold Yeast Two-Hybrid System). In accordance with the *Saccharomyces* Genome Database members of the *CDK8* module, *SSN8/CNC1/UME3/SRB11*, *SSN3/CDK8/UME5/SRB10*, *SRB8/MED12/SSN5* and *SSN2/MED13/UME2/SRB9*, will use *SSN8/CNC1*, *SSN3/CDK8*, *SRB8/MED12*, and *SSN2/MED13* gene designations, respectively.

Plasmids used in this study are listed in Table S2. Details are available upon request. The Gal4-BD and Gal4-AD fusion plasmids were constructed by amplifying alleles from genomic DNA into pAS2 [119] and pACT2-T7 respectively [21]. The Ksp1-GFP plasmids were constructed by first PCR-cloning the wild-type *KSP1* allele from RSY10 and ligating into pRS316. The *Ksp1*^{K47D} mutation was then introduced using site-directed mutagenesis (Quick Change Kit, New England Biolabs). The *ksp1*[*AIMΔ1*] and *ksp1*[*AIMΔ1,2*] plasmids were made as follows. First, *AIM1* (1022–1025) was simultaneously deleted and tagged with 9MYC in RSY10 using PCR replacement methodology to create RSY2742. PCR-cloning was then used to move *ksp1*[*AIMΔ1*]-9MYC into pRS316 [120] creating pSH37. Site-directed mutagenesis was then used to delete *AIM2* (aa167–172) in pSH37 creating pSH38. The *KSP1* Y2H subclones were constructed from PCR-cloning of wild-type *KSP1* from RSY10 into Gal4-BD plasmid. The C terminal subclone (pSH35) was then mutated using site-directed mutagenesis to replace leucine 1025 with an alanine residue. Site-directed mutagenesis was also used to replace tyrosine 49 and leucine 50 with alanine residues in GFP-Atg8 to create the Atg8[LDS] allele (pSH36). All constructs were verified by

sequencing. The integrating *PHO8-BFP* [121] plasmid was a gift from J. Nunnari, University of California, Davis, and was linearized using *BstEII* [121]. The Nup49-mCherry plasmid (Lep752) was a gift from K. Madura, Rutgers University. The *CUP1pAtg8-mCherry* plasmid [122] was a gift from D. Klionsky, The University of Michigan at Ann Harbor.

Cell growth

Yeast cells were grown in either rich, nonselective medium (YPDA: 2% [w:v] glucose, 2% w:v Bacto peptone, 1% w:v yeast extract, 0.001% w:v adenine sulfate) or synthetic minimal dextrose medium (SD: 0.17% w:v yeast nitrogen base without amino acids and ammonium sulfate, 0.5% w:v ammonium sulfate, 1× supplement mixture of amino acids, 2% w:v glucose) allowing plasmid selection as previously described [123–127]. For nitrogen-starvation experiments, cells were grown to mid-log in SD medium, spun down, washed, and resuspended in SD-N media (0.17% w:v yeast nitrogen base without amino acids, 0.17% w:v yeast nitrogen base without amino acids) for indicated time points. For rapamycin-treated cells, the cells were grown to mid-log phase ($\sim 6 \times 10^6$ cells/ml) in 2% glucose media, selecting for plasmids when appropriate before directly adding rapamycin (Biovision, 1746-1); dissolved in 10% Tween 20 (VWR, 0777-1 L) 90% ethanol.

Cellular assays

For Y2H assays, three biological replicates containing a Gal4-binding domain construct (pAS2 backbone) and a Gal4-activating domain construct (Gal4-AD-T7) were plated on medium selecting for plasmid maintenance (*-LEU*, *-TRP*). Interaction between proteins was monitored by selection on *-LEU*, *-TRP* *-ADE*, *-HIS* plates for 3 days at 30°C. To make the activation of *HIS3* more stringent, 3-aminotriazole (3-AT; Sigma, A8056-100 G) was supplemented into the above media at the concentrations indicated in the text. Activation of the two other reporter genes, *AURI-C* and *MEL1*, was monitored by the addition of 200 ng/mL aureobasidin A (Takara, 630466) and 40 ug/mL of X-alpha-Gal (GoldBio, XA250) respectively. The nitrogen starvation viability assays were executed in biological triplicate exactly as described [22]. Following staining with phloxine B (Millipore Sigma, P2759), 30000 cells were counted per timepoint using fluorescence-activated cell analysis (FACs). *P* values were determined using the unpaired Student's *t*-test. Data are mean \pm standard deviation.

Western blot assays, co-immunoprecipitation and GFP affinity isolation

Quantitative western blot analysis and co-immunoprecipitation assays were executed exactly as described [21]. Ksp1-GFP affinity-isolation assays were executed as follows. One mg of protein extract was made as described [21] and mixed with Chromotek GFP-Trap agarose beads (prepared as outlined by the manufacturer; Proteintech, gta). After 1 h rotating at 4°C, the beads were washed with IP wash buffer as described for co-IPs [21] with the addition of

0.05% Triton X-100 (Bio-Rad, 1610407). They were then analyzed as described for co-IPs. Antibodies used for western blot analysis were anti-Pgk1 (ThermoFisher, 459250), anti-MYC (EMD Millipore, 05-724), anti-HA (Abcam, AB9110), anti-GFP (Wako, 012-22541).

All protein degradation assays were performed in triplicate. Standard deviation and significance were calculated from the mean \pm standard deviation using GraphPad Prism 7. For quantification of degradation kinetics, band intensities of each time point were measured using an iBright CL1500 Imaging system (ThermoFisher). This value was first divided by unstressed, T = 0 band intensity. These values were then divided by Pgk1 loading band intensity values which were also normalized to their T = 0 intensities. Two-way ANOVAs were performed to determine the significance between every genotype and time point. The P-values shown are relative to wild-type T = 4 time points. This information was used to determine the line of best fit that was calculated by GraphPad Prism 7. Protein half-life was extrapolated using linear regression analysis, where 1.7 (log of 50, half of 100%) was used as the y value in the slope-intercept form equation. All representative results included at least two independent biological experiments. P values were generated from Prism GraphPad using unpaired ANOVA tests; NS $P \geq 0.05$; * $P \leq 0.05$, ** $P \leq 0.005$; *** $P \leq 0.001$; **** $P \leq 0.0001$. All error bars indicate mean \pm SD.

Fluorescence microscopy

For all microscopy experiments, cells were grown to mid-log, washed, and resuspended in SD-N for the time points indicated. Except for Figure 2B, deconvolved images were obtained using a Nikon microscope (Model E800) with a 100 \times objective using 1.2 \times camera magnification (Plan Fluor Oil, NA 1.3) and a CCD camera (Hamamatsu Model C4742). Data were collected using NIS software and processed using Image Pro software. All images of individual cells were optically sectioned (0.2- μ m slices at 0.3 μ m spacing) and deconvolved, and slices were collapsed to visualize the entire fluorescent signal within the cell. Linear quantification analysis was measured using the Image Pro software. The vacuoles were visualized in live cells either using mCherry-tagged Vph1, Pho8-BFP or staining with CMAC (Thermo, C2110; 100 μ M) as described [21]. In Figure 2B a Keyence BZ-X710 fluorescence microscope with a 100 \times objective with 1.0 \times camera magnification (PlanApo λ Oil, NA 1.45) and a CCD camera was used. The images were deconvolved using BZ-X Analyzer software.

Modeling

The ClusPro 2.0 protein-protein docking server [73,74] was used to simulate rigid body docking between Atg8 (PDB structure ID: 6WY6, chain A) and Ksp1 AIM domains (generated by AlphaFold [75,76]). For the simulations, Atg8 was set as the “receptor”, AlphaFold Ksp1 AIM domain.pdb files were uploaded as the “ligand”, and no advanced options were adjusted. Mutagenesis to the Ksp1 AIM domains was done using PyMol’s (PyMol.org) built-in protein mutagenesis

function with no additional modifications to the application’s mutagenesis parameters. Mutated structures were exported as .pdb files and re-tested using the ClusPro 2.0 server. Analysis of simulation files to determine interaction residues and interfaces was completed using the Protein interfaces, surfaces, and assemblies service PISA at the European Bioinformatics Institute (http://www.ebi.ac.uk/pdbe/prot_int/pistart.html, [120]). All ClusPro 2.0 generated models were uploaded to PISA as coordinate files, allowing for the identification of interfaces and a breakdown of interacting residues (hydrogen bonds, salt bridges, covalent bonds, and disulfide bonds). To analyze the localization of Ksp1 AIM domains/variants with regard to Atg8, models were imported into PyMol. Distribution percentages were completed based on three general localization interfaces of the AIM domains (based on Atg8 orientation utilized in the modeling images): at the LDS pocket of Atg8, above the LDS pocket, and below the LDS pocket. Images were created in PyMol. For modeling images, presented models represent only one model of many (30 for AIM1, up to 15 for AIM2 – difference due to protein-protein docking results). The models chosen are representative of the general behavior or trends shared among individual AIMs and variants.

Statistical analysis

All representative results included at least three independent biological experiments. P values were generated from Prism GraphPad using unpaired Student’s t-tests. For all figures NS $P \geq 0.05$; * $P \leq 0.05$, ** $P \leq 0.005$; *** $P \leq 0.001$; **** $P \leq 0.0001$. All error bars indicate mean \pm SD. If the error between all biological replicates was less than log 0.05, then no error bars were generated using GraphPad Prism 7. Protein levels were quantification exactly as previously described [21]. P-values shown are relative to wild-type T = 4 time points.

Acknowledgements

We thank P. Herman, K. Madura, D. Klionsky, and J. Nunnari for strains and plasmids. We especially thank the members of the Strich and Cooper laboratories for the critical reading of this manuscript.

Disclosure statement

No potential conflict of interest was reported by the author(s).

Funding

This work was supported by the New Jersey Health Foundation [PC-11-22] awarded to K.F.C. Additional support was provided by the New Jersey Health Foundation [PC-41-22], and the Osteopathic Heritage Foundation [OHFE-F-2022-27] to R. S.

ORCID

Katrina F. Cooper  <http://orcid.org/0000-0003-4619-7534>

References

- [1] Dikic I. Proteasomal and autophagic degradation systems. *Annu Rev Biochem.* 2017 Jun 20;86(1):193–224. doi: [10.1146/annurev-biochem-061516-044908](https://doi.org/10.1146/annurev-biochem-061516-044908)
- [2] Gubas A, Dikic I. A guide to the regulation of selective autophagy receptors. *FEBS J.* 2022 Jan;289(1):75–89. doi: [10.1111/febs.15824](https://doi.org/10.1111/febs.15824)
- [3] Levine B, Kroemer G. Biological functions of autophagy genes: a disease perspective. *Cell.* 2019 Jan 10;176(1–2):11–42. doi: [10.1016/j.cell.2018.09.048](https://doi.org/10.1016/j.cell.2018.09.048)
- [4] Hetz C, Saxena S. ER stress and the unfolded protein response in neurodegeneration. *Nat Rev Neurol.* 2017 Aug;13(8):477–491. doi: [10.1038/nrneuro.2017.99](https://doi.org/10.1038/nrneuro.2017.99)
- [5] Gonzalez-Teuber V, Albert-Gasco H, Auyeung VC, et al. Small molecules to improve ER proteostasis in disease. *Trends Pharmacol Sci.* 2019 Sep;40(9):684–695. doi: [10.1016/j.tips.2019.07.003](https://doi.org/10.1016/j.tips.2019.07.003)
- [6] Lawrence RE, Zoncu R. The lysosome as a cellular centre for signalling, metabolism and quality control. *Nat Cell Biol.* 2019 Feb;21(2):133–142. doi: [10.1038/s41556-018-0244-7](https://doi.org/10.1038/s41556-018-0244-7)
- [7] Dikic I, Elazar Z. Mechanism and medical implications of mammalian autophagy. *Nat Rev Mol Cell Biol.* 2018 Jun;19(6):349–364. doi: [10.1038/s41580-018-0003-4](https://doi.org/10.1038/s41580-018-0003-4)
- [8] Hollenstein DM, Kraft C. Autophagosomes are formed at a distinct cellular structure. *Curr Opin Cell Biol.* 2020 Mar 20;65:50–57. doi: [10.1016/j.ccb.2020.02.012](https://doi.org/10.1016/j.ccb.2020.02.012)
- [9] Gonzalez A, Hall MN. Nutrient sensing and TOR signaling in yeast and mammals. *EMBO J.* 2017 Feb 15;36(4):397–408. doi: [10.15252/embj.201696010](https://doi.org/10.15252/embj.201696010)
- [10] Delorme-Axford E, Klionsky DJ. Transcriptional and post-transcriptional regulation of autophagy in the yeast *Saccharomyces cerevisiae*. *J Biol Chem.* 2018 Jan 25;293(15):5396–5403. doi: [10.1074/jbc.R117.804641](https://doi.org/10.1074/jbc.R117.804641)
- [11] Johansen T, Lamark T. Selective autophagy: ATG8 family proteins, LIR motifs and cargo receptors. *J Mol Biol.* 2020 Jan 3;432(1):80–103. doi: [10.1016/j.jmb.2019.07.016](https://doi.org/10.1016/j.jmb.2019.07.016)
- [12] Kirkin V, Rogov VV, Rogov VV. A diversity of selective autophagy receptors determines the specificity of the autophagy pathway. *Mol Cell.* 2019 Oct 17;76(2):268–285. doi: [10.1016/j.molcel.2019.09.005](https://doi.org/10.1016/j.molcel.2019.09.005)
- [13] Rogov V, Dotsch V, Johansen T, et al. Interactions between autophagy receptors and ubiquitin-like proteins form the molecular basis for selective autophagy. *Mol Cell.* 2014 Jan 23;53(2):167–178. doi: [10.1016/j.molcel.2013.12.014](https://doi.org/10.1016/j.molcel.2013.12.014)
- [14] Stolz A, Ernst A, Dikic I. Cargo recognition and trafficking in selective autophagy. *Nat Cell Biol.* 2014 Jun;16(6):495–501. doi: [10.1038/ncb2979](https://doi.org/10.1038/ncb2979)
- [15] Farre JC, Subramani S. Mechanistic insights into selective autophagy pathways: lessons from yeast. *Nat Rev Mol Cell Biol.* 2016 Sep;17(9):537–552. doi: [10.1038/nrm.2016.74](https://doi.org/10.1038/nrm.2016.74)
- [16] Marshall RS, Hua Z, Mali S, et al. ATG8-binding UIM proteins define a New class of autophagy adaptors and receptors. *Cell.* 2019 Apr 18;177(3):766–781 e24. doi: [10.1016/j.cell.2019.02.009](https://doi.org/10.1016/j.cell.2019.02.009)
- [17] Martens S, Behrends C. Molecular mechanisms of selective autophagy. *J Mol Biol.* 2020 Jan 3;432(1):1–2. doi: [10.1016/j.jmb.2019.11.010](https://doi.org/10.1016/j.jmb.2019.11.010)
- [18] Shintani T, Klionsky DJ. Autophagy in health and disease: a double-edged sword. *Science.* 2004 Nov 5;306(5698):990–995. doi: [10.1126/science.1099993](https://doi.org/10.1126/science.1099993)
- [19] Lu K, Psakhye I, Jentsch S. Autophagic clearance of polyQ proteins mediated by ubiquitin-Atg8 adaptors of the conserved CUET protein family. *Cell.* 2014 Jul 31;158(3):549–563. doi: [10.1016/j.cell.2014.05.048](https://doi.org/10.1016/j.cell.2014.05.048)
- [20] Marshall RS, McLoughlin F, Vierstra RD. Autophagic turnover of inactive 26S proteasomes in yeast is directed by the ubiquitin receptor Cue5 and the Hsp42 chaperone. *Cell Rep.* 2016 Aug 9;16(6):1717–1732. doi: [10.1016/j.celrep.2016.07.015](https://doi.org/10.1016/j.celrep.2016.07.015)
- [21] Hanley SE, Willis SD, Cooper KF. Snx4-assisted vacuolar targeting of transcription factors defines a new autophagy pathway for controlling ATG expression. *Autophagy.* 2021 Nov;17(11):3547–3565. doi: [10.1080/15548627.2021.1877934](https://doi.org/10.1080/15548627.2021.1877934)
- [22] Willis SD, Hanley SE, Beishke T, et al. Ubiquitin–proteasome-mediated cyclin C degradation promotes cell survival following nitrogen starvation. *Mol Biol Cell.* 2020 May 1;31(10):1015–1031. doi: [10.1091/mbc.E19-11-0622](https://doi.org/10.1091/mbc.E19-11-0622)
- [23] Willis SD, Hanley SE, Doyle SJ, et al. Cyclin C-Cdk8 kinase phosphorylation of Rim15 prevents the aberrant activation of stress response genes. *Front Cell Dev Biol.* 2022;10:867257. doi: [10.3389/fcell.2022.867257](https://doi.org/10.3389/fcell.2022.867257)
- [24] Friedson B, Cooper KF. Cdk8 kinase module: a mediator of life and death decisions in times of stress. *Microorganisms.* 2021;9(10):2152. doi: [10.3390/microorganisms9102152](https://doi.org/10.3390/microorganisms9102152)
- [25] Noble KN, Tran EJ, Alcazar-Roman AR, et al. The Dbp5 cycle at the nuclear pore complex during mRNA export II: nucleotide cycling and mRNP remodeling by Dbp5 are controlled by Nup159 and Gle1. *Genes Dev.* 2011 May 15;25(10):1065–1077. doi: [10.1101/gad.2040611](https://doi.org/10.1101/gad.2040611)
- [26] Nice DC, Sato TK, Stromhaug PE, et al. Cooperative binding of the cytoplasm to vacuole targeting pathway proteins, Cvt13 and Cvt20, to phosphatidylinositol 3-phosphate at the pre-autophagosomal structure is required for selective autophagy. *J Biol Chem.* 2002 Aug 16;277(33):30198–30207. doi: [10.1074/jbc.M204736200](https://doi.org/10.1074/jbc.M204736200)
- [27] Hanley SE, Cooper KF. Sorting nexins in protein homeostasis. *Cells.* 2020 Dec 24;10(1):17. doi: [10.3390/cells10010017](https://doi.org/10.3390/cells10010017)
- [28] Fleischmann M, Stagljar I, Aebi M. Allele-specific suppression of a *Saccharomyces cerevisiae* prp20 mutation by overexpression of a nuclear serine/threonine protein kinase. *Mol Genet.* 1996 Mar 20;250(5):614–625. doi: [10.1007/BF02174449](https://doi.org/10.1007/BF02174449)
- [29] Mace K, Krakowiak J, El-Samad H, et al. Multi-kinase control of environmental stress responsive transcription. *PLoS One.* 2020;15(3):e0230246. doi: [10.1371/journal.pone.0230246](https://doi.org/10.1371/journal.pone.0230246)
- [30] Bharucha N, Ma J, Dobry CJ, et al. Analysis of the yeast kinome reveals a network of regulated protein localization during filamentous growth. *Mol Biol Cell.* 2008 Jul;19(7):2708–2717. doi: [10.1091/mbc.e07-11-1199](https://doi.org/10.1091/mbc.e07-11-1199)
- [31] Mutlu N, Sheidy DT, Hsu A, et al. A stress-responsive signaling network regulating pseudohyphal growth and ribonucleoprotein granule abundance in *Saccharomyces cerevisiae*. *Genetics.* 2019 Oct;213(2):705–720. doi: [10.1534/genetics.119.302538](https://doi.org/10.1534/genetics.119.302538)
- [32] Mitchell SF, Jain S, She M, et al. Global analysis of yeast mRNPs. *Nat Struct Mol Biol.* 2013 Jan;20(1):127–133. doi: [10.1038/nsmb.2468](https://doi.org/10.1038/nsmb.2468)
- [33] Jain S, Wheeler JR, Walters RW, et al. ATPase-modulated stress granules contain a diverse proteome and substructure. *Cell.* 2016 Jan 28;164(3):487–498. doi: [10.1016/j.cell.2015.12.038](https://doi.org/10.1016/j.cell.2015.12.038)
- [34] Laxman S, Tu BP, Arkowitz RA. Multiple TORC1-associated proteins regulate nitrogen starvation-dependent cellular differentiation in *Saccharomyces cerevisiae*. *PLoS One.* 2011;6(10):e26081. doi: [10.1371/journal.pone.0026081](https://doi.org/10.1371/journal.pone.0026081)
- [35] Umekawa M, Klionsky DJ. Ksp1 kinase regulates autophagy via the target of rapamycin complex 1 (TORC1) pathway. *J Biol Chem.* 2012 May 11;287(20):16300–16310. doi: [10.1074/jbc.M112.344952](https://doi.org/10.1074/jbc.M112.344952)
- [36] Huber A, Bodenmiller B, Uotila A, et al. Characterization of the rapamycin-sensitive phosphoproteome reveals that Sch9 is a central coordinator of protein synthesis. *Genes Dev.* 2009 Aug 15;23(16):1929–1943. doi: [10.1101/gad.532109](https://doi.org/10.1101/gad.532109)
- [37] Oliveira AP, Ludwig C, Zampieri M, et al. Dynamic phosphoproteomics reveals TORC1-dependent regulation of yeast nucleotide and amino acid biosynthesis. *Sci Signal.* 2015 Apr 28;8(374):rs4. doi: [10.1126/scisignal.2005768](https://doi.org/10.1126/scisignal.2005768)
- [38] Soulard A, Cremonesi A, Moes S, et al. The rapamycin-sensitive phosphoproteome reveals that TOR controls protein kinase a toward some but not all substrates. *Mol Biol Cell.* 2010 Oct 1;21(19):3475–3486. doi: [10.1091/mbc.e10-03-0182](https://doi.org/10.1091/mbc.e10-03-0182)
- [39] Ptacek J, Devgan G, Michaud G, et al. Global analysis of protein phosphorylation in yeast. *Nature.* 2005 Dec 1;438(7068):679–684. doi: [10.1038/nature04187](https://doi.org/10.1038/nature04187)
- [40] Chang Y, Huh WK. Ksp1-dependent phosphorylation of eIF4G modulates post-transcriptional regulation of specific mRNAs

- under glucose deprivation conditions. *Nucleic Acids Res.* 2018 Apr 6;46(6):3047–3060. doi: [10.1093/nar/gky097](https://doi.org/10.1093/nar/gky097)
- [41] Stieg DC, Willis SD, Ganesan V, et al. A complex molecular switch directs stress-induced cyclin C nuclear release through SCF Grr1-mediated degradation of Med13. *Mol Biol Cell.* 2018 Feb 1;29(3):363–375. doi: [10.1091/mbc.E17-08-0493](https://doi.org/10.1091/mbc.E17-08-0493)
- [42] Takeshige K, Baba M, Tsuboi S, et al. Autophagy in yeast demonstrated with proteinase-deficient mutants and conditions for its induction. *J Cell Bio.* 1992 Oct;119(2):301–311. doi: [10.1083/jcb.119.2.301](https://doi.org/10.1083/jcb.119.2.301)
- [43] Den Hazel HB V, Kielland-Brandt MC, Winther JR. Review: biosynthesis and function of yeast vacuolar proteases. *Yeast.* 1996 Jan;12(1):1–16. doi: [10.1002/\(SICI\)1097-0061\(199601\)12:1<1:AID-YEA902>3.0.CO;2-N](https://doi.org/10.1002/(SICI)1097-0061(199601)12:1<1:AID-YEA902>3.0.CO;2-N)
- [44] Xie Z, Nair U, Klionsky DJ, et al. Atg8 controls phagophore expansion during autophagosome formation. *Mol Biol Cell.* 2008 Aug;19(8):3290–3298. doi: [10.1091/mbc.e07-12-1292](https://doi.org/10.1091/mbc.e07-12-1292)
- [45] Tanida I, Mizushima N, Kiyooka M, et al. Apg7p/Cvt2p: a novel protein-activating enzyme essential for autophagy. *Mol Biol Cell.* 1999 May;10(5):1367–1379. doi: [10.1091/mbc.10.5.1367](https://doi.org/10.1091/mbc.10.5.1367)
- [46] Kotani T, Kirisako H, Koizumi M, et al. The Atg2-Atg18 complex tethers pre-autophagosomal membranes to the endoplasmic reticulum for autophagosome formation. *Proc Natl Acad Sci U S A.* 2018 Oct 9;115(41):10363–10368. doi: [10.1073/pnas.1806727115](https://doi.org/10.1073/pnas.1806727115)
- [47] Xu H, Jun Y, Thompson J, et al. HOPS prevents the disassembly of trans-SNARE complexes by Sec17p/Sec18p during membrane fusion. *EMBO J.* 2010 Jun 16;29(12):1948–1960. doi: [10.1038/emboj.2010.97](https://doi.org/10.1038/emboj.2010.97)
- [48] D'Agostino M, Risselada HJ, Lurick A, et al. A tethering complex drives the terminal stage of SNARE-dependent membrane fusion. *Nature.* 2017 Nov 30;551(7682):634–638. doi: [10.1038/nature24469](https://doi.org/10.1038/nature24469)
- [49] Lőrincz P, Juhász G. Autophagosome-lysosome fusion. *J Mol Biol.* 2020 April 03;432(8):2462–2482.
- [50] Dosztanyi Z, Csizmok V, Tompa P, et al. Iupred: web server for the prediction of intrinsically unstructured regions of proteins based on estimated energy content. *Bioinformatics.* 2005 Aug 15;21(16):3433–3434. doi: [10.1093/bioinformatics/bti541](https://doi.org/10.1093/bioinformatics/bti541)
- [51] Mészáros B, Erdős G, Dosztányi Z. IUPred2A: context-dependent prediction of protein disorder as a function of redox state and protein binding. *Nucleic Acids Res.* 2018;46(W1):W329–W337. doi: [10.1093/nar/gky384](https://doi.org/10.1093/nar/gky384)
- [52] Erdos G, Pajkos M, Dosztanyi Z. IUPred3: prediction of protein disorder enhanced with unambiguous experimental annotation and visualization of evolutionary conservation. *Nucleic Acids Res.* 2021 Jul 2;49(W1):W297–W303. doi: [10.1093/nar/gkab408](https://doi.org/10.1093/nar/gkab408)
- [53] Barz S, Kriegenburg F, Sánchez-Martín P, et al. Small but mighty: Atg8s and rabs in membrane dynamics during autophagy. *Biochim Biophys Acta (BBA) - Mol Cell Res.* 2021 Aug 1;1868(9):119064. doi: [10.1016/j.bbamcr.2021.119064](https://doi.org/10.1016/j.bbamcr.2021.119064)
- [54] Dyson HJ, Wright PE. Intrinsically unstructured proteins and their functions. *Nat Rev Mol Cell Biol.* 2005 Mar;6(3):197–208. doi: [10.1038/nrml589](https://doi.org/10.1038/nrml589)
- [55] Mei Y, Su M, Soni G, et al. Intrinsically disordered regions in autophagy proteins. *Proteins.* 2014 Apr;82(4):565–578. doi: [10.1002/prot.24424](https://doi.org/10.1002/prot.24424)
- [56] Jacomin AC, Samavedam S, Promponas V, et al. iLIR database: a web resource for LIR motif-containing proteins in eukaryotes. *Autophagy.* 2016 Oct 2;12(10):1945–1953. doi: [10.1080/15548627.2016.1207016](https://doi.org/10.1080/15548627.2016.1207016)
- [57] Meszaros B, Simon I, Dosztanyi Z. Prediction of protein binding regions in disordered proteins. *PLoS Comput Biol.* 2009 May;5(5):e1000376. doi: [10.1371/journal.pcbi.1000376](https://doi.org/10.1371/journal.pcbi.1000376)
- [58] Dosztanyi Z, Meszaros B, Simon I. ANCHOR: web server for predicting protein binding regions in disordered proteins. *Bioinformatics.* 2009 Oct 15;25(20):2745–2746. doi: [10.1093/bioinformatics/btp518](https://doi.org/10.1093/bioinformatics/btp518)
- [59] Ramos PC, Hockendorff J, Johnson ES, et al. Ump1p is required for proper maturation of the 20S proteasome and becomes its substrate upon completion of the assembly. *Cell.* 1998;92(4):489–499. doi: [10.1016/S0092-8674\(00\)80942-3](https://doi.org/10.1016/S0092-8674(00)80942-3)
- [60] Czabotar PE, Westphal D, Dewson G, et al. Bax crystal structures reveal how BH3 domains activate Bax and nucleate its oligomerization to induce apoptosis. *Cell.* 2013 Jan 31;152(3):519–531. doi: [10.1016/j.cell.2012.12.031](https://doi.org/10.1016/j.cell.2012.12.031)
- [61] Uekusa Y, Okawa K, Yagi-Utsumi M, et al. Backbone (1)H, (1)(3)C and (1)(5)N assignments of yeast Ump1, an intrinsically disordered protein that functions as a proteasome assembly chaperone. *Biomol NMR Assign.* 2014 Oct;8(2):383–386. doi: [10.1007/s12104-013-9523-1](https://doi.org/10.1007/s12104-013-9523-1)
- [62] Li X, Kusmierczyk AR, Wong P, et al. Beta-subunit appendages promote 20S proteasome assembly by overcoming an Ump1-dependent checkpoint. *EMBO J.* 2007 May 2;26(9):2339–2349. doi: [10.1038/sj.emboj.7601681](https://doi.org/10.1038/sj.emboj.7601681)
- [63] Loos B, du Toit A, Hofmeyr JH. Defining and measuring autophagosome flux-concept and reality. *Autophagy.* 2014;10(11):2087–2096. doi: [10.4161/15548627.2014.973338](https://doi.org/10.4161/15548627.2014.973338)
- [64] Suzuki K, Kirisako T, Kamada Y, et al. The pre-autophagosomal structure organized by concerted functions of APG genes is essential for autophagosome formation. *EMBO J.* 2001 Nov 1;20(21):5971–5981. doi: [10.1093/emboj/20.21.5971](https://doi.org/10.1093/emboj/20.21.5971)
- [65] Delorme-Axford E, Guimaraes RS, Reggiori F, et al. The yeast *Saccharomyces cerevisiae*: an overview of methods to study autophagy progression. *Methods.* 2015 Mar;75:3–12.
- [66] Noda NN, Kumeta H, Nakatogawa H, et al. Structural basis of target recognition by Atg8/LC3 during selective autophagy. *Genes Cells.* 2008 Dec;13(12):1211–1218. doi: [10.1111/j.1365-2443.2008.01238.x](https://doi.org/10.1111/j.1365-2443.2008.01238.x)
- [67] Noda NN, Ohsumi Y, Inagaki F. Atg8-family interacting motif crucial for selective autophagy. *FEBS Lett.* 2010 Apr 2;584(7):1379–1385. doi: [10.1016/j.febslet.2010.01.018](https://doi.org/10.1016/j.febslet.2010.01.018)
- [68] Ho KH, Chang HE, Huang WP. Mutation at the cargo-receptor binding site of Atg8 also affects its general autophagy regulation function. *Autophagy.* 2009 May;5(4):461–471. doi: [10.4161/auto.5.4.7696](https://doi.org/10.4161/auto.5.4.7696)
- [69] Kirisako T, Ichimura Y, Okada H, et al. The reversible modification regulates the membrane-binding state of Apg8/Aut7 essential for autophagy and the cytoplasm to vacuole targeting pathway. *J Cell Bio.* 2000 Oct 16;151(2):263–276. doi: [10.1083/jcb.151.2.263](https://doi.org/10.1083/jcb.151.2.263)
- [70] Hutchins MU, Klionsky DJ. Vacuolar localization of oligomeric alpha-mannosidase requires the cytoplasm to vacuole targeting and autophagy pathway components in *Saccharomyces cerevisiae*. *J Biol Chem.* 2001 Jun 8;276(23):20491–20498. doi: [10.1074/jbc.M101150200](https://doi.org/10.1074/jbc.M101150200)
- [71] Alemu EA, Lamark T, Torgersen KM, et al. ATG8 family proteins act as scaffolds for assembly of the ULK complex: sequence requirements for LC3-interacting region (LIR) motifs. *J Biol Chem.* 2012 Nov 16;287(47):39275–39290. doi: [10.1074/jbc.M112.378109](https://doi.org/10.1074/jbc.M112.378109)
- [72] Kalvari I, Tsompanis S, Mulakkal NC, et al. iLIR: a web resource for prediction of Atg8-family interacting proteins. *Autophagy.* 2014 May;10(5):913–925. doi: [10.4161/auto.28260](https://doi.org/10.4161/auto.28260)
- [73] Kozakov D, Hall DR, Xia B, et al. The ClusPro web server for protein-protein docking. *Nat Protoc.* 2017 Feb;12(2):255–278. doi: [10.1038/nprot.2016.169](https://doi.org/10.1038/nprot.2016.169)
- [74] Desta IT, Porter KA, Xia B, et al. Performance and its limits in rigid body protein-protein docking. *Structure.* 2020 Sep 1;28(9):1071–1081 e3. doi: [10.1016/j.str.2020.06.006](https://doi.org/10.1016/j.str.2020.06.006)
- [75] Varadi M, Anyango S, Deshpande M, et al. AlphaFold protein structure database: massively expanding the structural coverage of protein-sequence space with high-accuracy models. *Nucleic Acids Res.* 2021;50(D1):D439–D444. doi: [10.1093/nar/gkab1061](https://doi.org/10.1093/nar/gkab1061)
- [76] Jumper J, Evans R, Pritzel A, et al. Highly accurate protein structure prediction with AlphaFold. *Nature.* 2021 Aug;596(7873):583–589. doi: [10.1038/s41586-021-03819-2](https://doi.org/10.1038/s41586-021-03819-2)
- [77] Suzuki K, Kondo C, Morimoto M, et al. Selective transport of alpha-mannosidase by autophagic pathways: identification of

- a novel receptor, Atg34p. *J Biol Chem.* 2010 Sep 24;285(39):30019–30025. doi: [10.1074/jbc.M110.143511](https://doi.org/10.1074/jbc.M110.143511)
- [78] Sora V, Kumar M, Maiani E, et al. Structure and dynamics in the ATG8 family from Experimental to Computational Techniques. *Front Cell Dev Biol.* 2020;8:420. doi: [10.3389/fcell.2020.00420](https://doi.org/10.3389/fcell.2020.00420)
- [79] Scott SV, Guan J, Hutchins MU, et al. Cvt19 is a receptor for the cytoplasm-to-vacuole targeting pathway. *Mol Cell.* 2001 Jun;7(6):1131–1141. doi: [10.1016/S1097-2765\(01\)00263-5](https://doi.org/10.1016/S1097-2765(01)00263-5)
- [80] Sawa-Makarska J, Abert C, Romanov J, et al. Cargo binding to Atg19 unmasks additional Atg8 binding sites to mediate membrane-cargo apposition during selective autophagy. *Nat Cell Biol.* 2014 May;16(5):425–433. doi: [10.1038/ncb2935](https://doi.org/10.1038/ncb2935)
- [81] Abert C, Kontaxis G, Martens S. Accessory interaction motifs in the Atg19 cargo receptor Enable strong binding to the clustered ubiquitin-related Atg8 protein. *J Biol Chem.* 2016 Sep 2;291(36):18799–18808. doi: [10.1074/jbc.M116.736892](https://doi.org/10.1074/jbc.M116.736892)
- [82] Liu L, Levin DE, Lew DJ. Intracellular mechanism by which genotoxic stress activates yeast SAPK Mpk1. *Mol Biol Cell.* 2018 Nov 15;29(23):2898–2909. doi: [10.1091/mbc.E18-07-0441](https://doi.org/10.1091/mbc.E18-07-0441)
- [83] Yorimitsu T, Klionsky DJ. Atg11 links cargo to the vesicle-forming machinery in the cytoplasm to vacuole targeting pathway. *Mol Biol Cell.* 2005 Apr;16(4):1593–1605. doi: [10.1091/mbc.e04-11-1035](https://doi.org/10.1091/mbc.e04-11-1035)
- [84] Suzuki SW, Emr SD. Membrane protein recycling from the vacuole/lysosome membrane. *J Cell Bio.* 2018 May 7;217(5):1623–1632. doi: [10.1083/jcb.201709162](https://doi.org/10.1083/jcb.201709162)
- [85] Zientara-Rytter K, Subramani S. Mechanistic insights into the role of Atg11 in selective autophagy. *J Mol Biol.* 2020 Jan 3;432(1):104–122. doi: [10.1016/j.jmb.2019.06.017](https://doi.org/10.1016/j.jmb.2019.06.017)
- [86] Kawamata T, Kamada Y, Kabeya Y, et al. Organization of the pre-autophagosomal structure responsible for autophagosome formation. *Mol Biol Cell.* 2008 May;19(5):2039–2050. doi: [10.1091/mbc.e07-10-1048](https://doi.org/10.1091/mbc.e07-10-1048)
- [87] Yamamoto H, Fujioka Y, Suzuki SW, et al. The intrinsically disordered protein Atg13 mediates supramolecular assembly of autophagy initiation complexes. *Dev Cell.* 2016 Jul 11;38(1):86–99. doi: [10.1016/j.devcel.2016.06.015](https://doi.org/10.1016/j.devcel.2016.06.015)
- [88] Kawamata T, Kamada Y, Suzuki K, et al. Characterization of a novel autophagy-specific gene, ATG29. *Biochem Biophys Res Commun.* 2005 Dec 30;338(4):1884–1889. doi: [10.1016/j.bbrc.2005.10.163](https://doi.org/10.1016/j.bbrc.2005.10.163)
- [89] Caufield JH, Sakhawalkar N, Uetz P. A comparison and optimization of yeast two-hybrid systems. *Methods.* 2012 Dec;58(4):317–324. doi: [10.1016/j.ymeth.2012.12.001](https://doi.org/10.1016/j.ymeth.2012.12.001)
- [90] Okamoto K, Kondo-Okamoto N, Ohsumi Y. Mitochondria-anchored receptor Atg32 mediates degradation of mitochondria via selective autophagy. *Dev Cell.* 2009 Jul;17(1):87–97. doi: [10.1016/j.devcel.2009.06.013](https://doi.org/10.1016/j.devcel.2009.06.013)
- [91] Suzuki H, Osawa T, Fujioka Y, et al. Structural biology of the core autophagy machinery. *Curr Opin Struct Biol.* 2017 Apr;43:10–17.
- [92] Kanki T, Wang K, Cao Y, et al. Atg32 is a mitochondrial protein that confers selectivity during mitophagy. *Dev Cell.* 2009 Jul;17(1):98–109. doi: [10.1016/j.devcel.2009.06.014](https://doi.org/10.1016/j.devcel.2009.06.014)
- [93] Shpilka T, Welter E, Borovsky N, et al. Fatty acid synthase is preferentially degraded by autophagy upon nitrogen starvation in yeast. *Proc Natl Acad Sci U S A.* 2015 Feb 3;112(5):1434–1439. doi: [10.1073/pnas.1409476112](https://doi.org/10.1073/pnas.1409476112)
- [94] Deng Y, Qu Z, Naqvi NI, et al. The role of snx41-based pexophagy in magnaporthe development. *PLoS One.* 2013;8(11):e79128. doi: [10.1371/journal.pone.0079128](https://doi.org/10.1371/journal.pone.0079128)
- [95] Popelka H, Damasio A, Hinshaw JE, et al. Structure and function of yeast Atg20, a sorting nexin that facilitates autophagy induction. *Proc Natl Acad Sci U S A.* 2017 Nov 21;114(47):E10112–E10121. doi: [10.1073/pnas.1708367114](https://doi.org/10.1073/pnas.1708367114)
- [96] Galluzzi L, Baehrecke EH, Ballabio A, et al. Molecular definitions of autophagy and related processes. *EMBO J.* 2017 Jul 3;36(13):1811–1836. doi: [10.15252/embj.201796697](https://doi.org/10.15252/embj.201796697)
- [97] von Muhlinen N, Akutsu M, Ravenhill BJ, et al. LC3C, bound selectively by a noncanonical LIR motif in NDP52, is required for antibacterial autophagy. *Molecular Cell.* 2012 11;48(3):329–342. doi: [10.1016/j.molcel.2012.08.024](https://doi.org/10.1016/j.molcel.2012.08.024)
- [98] An H, Harper JW. Systematic analysis of ribophagy in human cells reveals bystander flux during selective autophagy. *Nat Cell Biol.* 2018 Feb 1;20(2):135–143.
- [99] Münch C, Dikic I. Hitchhiking on selective autophagy. *Nat Cell Biol.* 2018 Feb 1;20(2):122–124.
- [100] Mochida K, Oikawa Y, Kimura Y, et al. Receptor-mediated selective autophagy degrades the endoplasmic reticulum and the nucleus. *Nature.* 2015 Jun 18;522(7556):359–362. doi: [10.1038/nature14506](https://doi.org/10.1038/nature14506)
- [101] Farre JC, Manjithaya R, Mathewson RD, et al. PpAtg30 tags peroxisomes for turnover by selective autophagy. *Dev Cell.* 2008 Mar;14(3):365–376. doi: [10.1016/j.devcel.2007.12.011](https://doi.org/10.1016/j.devcel.2007.12.011)
- [102] Motley AM, Nuttall JM, Hettema EH. Pex3-anchored Atg36 tags peroxisomes for degradation in *Saccharomyces cerevisiae*. *EMBO J.* 2012 Jun 29;31(13):2852–2868. doi: [10.1038/emboj.2012.151](https://doi.org/10.1038/emboj.2012.151)
- [103] Farre JC, Burkenroad A, Burnett SF, et al. Phosphorylation of mitophagy and pexophagy receptors coordinates their interaction with Atg8 and Atg11. *EMBO Rep.* 2013 May;14(5):441–449. doi: [10.1038/embor.2013.40](https://doi.org/10.1038/embor.2013.40)
- [104] Nakatogawa H, Mochida K. Reticulophagy and nucleophagy: new findings and unsolved issues. *Autophagy.* 2015;11(12):2377–2378. doi: [10.1080/15548627.2015.1106665](https://doi.org/10.1080/15548627.2015.1106665)
- [105] Matscheko N, Mayrhofer P, Rao Y, et al. Atg11 tethers Atg9 vesicles to initiate selective autophagy. *PLoS Biol.* 2019 Jul;17(7):e3000377. doi: [10.1371/journal.pbio.3000377](https://doi.org/10.1371/journal.pbio.3000377)
- [106] Eickhorst C, Licheva M, Kraft C. Scaffold proteins in bulk and selective autophagy. *Prog Mol Biol Transl Sci.* 2020;172:15–35.
- [107] Liu X, Mao K, AYH Y, et al. The Atg17-Atg31-Atg29 complex coordinates with Atg11 to recruit the Vam7 SNARE and mediate autophagosome-vacuole fusion. *Curr Biol.* 2016 Jan 25;26(2):150–160. doi: [10.1016/j.cub.2015.11.054](https://doi.org/10.1016/j.cub.2015.11.054)
- [108] Hara T, Takamura A, Kishi C, et al. FIP200, a ULK-interacting protein, is required for autophagosome formation in mammalian cells. *J Cell Bio.* 2008 May 5;181(3):497–510. doi: [10.1083/jcb.200712064](https://doi.org/10.1083/jcb.200712064)
- [109] Zachari M, Ganley IG, Lane JD, et al. The mammalian ULK1 complex and autophagy initiation. *Essays Biochem.* 2017 Dec 12;61(6):585–596. doi: [10.1042/EBC20170021](https://doi.org/10.1042/EBC20170021)
- [110] Khakhina S, Cooper KF, Strich R, et al. Med13p prevents mitochondrial fission and programmed cell death in yeast through nuclear retention of cyclin C. *Mol Biol Cell.* 2014 Sep 15;25(18):2807–2816. doi: [10.1091/mbc.e14-05-0953](https://doi.org/10.1091/mbc.e14-05-0953)
- [111] Li YC, Chao TC, Kim HJ, et al. Structure and noncanonical Cdk8 activation mechanism within an argonaute-containing mediator kinase module. *Sci Adv.* 2021 Jan;7(3). doi: [10.1126/sciadv.abd4484](https://doi.org/10.1126/sciadv.abd4484)
- [112] Matsuyama H, Suzuki HI. Systems and synthetic microRNA Biology: from biogenesis to disease pathogenesis. *Int J Mol Sci.* 2019 Dec 24;21(1):132. doi: [10.3390/ijms21010132](https://doi.org/10.3390/ijms21010132)
- [113] Fabian MR, Sonenberg N. The mechanics of miRNA-mediated gene silencing: a look under the hood of miRISC. *Nat Struct Mol Biol.* 2012 June 01;19(6):586–593.
- [114] Sen GL, Blau HM. Argonaute 2/RISC resides in sites of mammalian mRNA decay known as cytoplasmic bodies. *Nat Cell Biol.* 2005 June 01;7(6):633–636.
- [115] Buchan JR. mRNA granules. *RNA Biol.* 2014 Aug 03;11(8):1019–1030.
- [116] Makino S, Kawamata T, Iwasaki S, et al. Selectivity of mRNA degradation by autophagy in yeast. *Nat Commun.* 2021 Apr 19;12(1):2316. doi: [10.1038/s41467-021-22574-6](https://doi.org/10.1038/s41467-021-22574-6)
- [117] Ronne H, Rothstein R. Mitotic sectored colonies: evidence of heteroduplex DNA formation during direct repeat recombination. *Proc Natl Acad Sci U S A.* 1988 Apr;85(8):2696–2700. doi: [10.1073/pnas.85.8.2696](https://doi.org/10.1073/pnas.85.8.2696)
- [118] Janke C, Magiera MM, Rathfelder N, et al. A versatile toolbox for PCR-based tagging of yeast genes: new fluorescent proteins, more markers and promoter substitution cassettes. *Yeast.* 2004 Aug;21(11):947–962. doi: [10.1002/yea.1142](https://doi.org/10.1002/yea.1142)
- [119] Wang R, Solomon MJ, Koepf DM. Identification of She3 as an SCF(Grr1) substrate in budding yeast. *PLoS One.* 2012;7(10):e48020. doi: [10.1371/journal.pone.0048020](https://doi.org/10.1371/journal.pone.0048020)

- [120] Sikorski RS, Hieter P. A system of shuttle vectors and yeast host strains designed for efficient manipulation of DNA in *Saccharomyces cerevisiae*. *Genet.* 1989;122(1):19–27. doi: [10.1093/genetics/122.1.19](https://doi.org/10.1093/genetics/122.1.19)
- [121] Graef M, Friedman JR, Graham C, et al. ER exit sites are physical and functional core autophagosome biogenesis components. *Mol Biol Cell.* 2013 Sep;24(18):2918–2931. doi: [10.1091/mbc.e13-07-0381](https://doi.org/10.1091/mbc.e13-07-0381)
- [122] Cebollero E, Reggiori F. Regulation of autophagy in yeast *Saccharomyces cerevisiae*. *Biochim Biophys Acta.* 2009 Sep;1793(9):1413–1421. doi: [10.1016/j.bbamcr.2009.01.008](https://doi.org/10.1016/j.bbamcr.2009.01.008)
- [123] Cooper KF, Mallory MJ, Smith JB, et al. Stress and developmental regulation of the yeast C-type cyclin Ume3p (Srb11p/Ssn8p). *EMBO J.* 1997 Aug 1;16(15):4665–4675. doi: [10.1093/emboj/16.15.4665](https://doi.org/10.1093/emboj/16.15.4665)
- [124] Strich R, Slater MR, Esposito RE. Identification of negative regulatory genes that govern the expression of early meiotic genes in yeast. *Proc Natl Acad Sci, USA.* 1989;86(24):10018–10022. doi: [10.1073/pnas.86.24.10018](https://doi.org/10.1073/pnas.86.24.10018)
- [125] Zubenko GS, Park FJ, Jones EW. Mutations in PEP4 locus of *Saccharomyces cerevisiae* block final step in maturation of two vacuolar hydrolases. *Proc Natl Acad Sci U S A.* 1983 Jan;80(2):510–514. doi: [10.1073/pnas.80.2.510](https://doi.org/10.1073/pnas.80.2.510)
- [126] Abeliovich H, Zhang C, Dunn WA Jr., et al. Chemical genetic analysis of Apg1 reveals a non-kinase role in the induction of autophagy. *Mol Biol Cell.* 2003 Feb;14(2):477–490. doi: [10.1091/mbc.e02-07-0413](https://doi.org/10.1091/mbc.e02-07-0413)
- [127] Wade Harper J, Adami GR, Wei N, et al. The p21 cdk-interacting protein Cip1 is a potent inhibitor of G1 cyclin-dependent kinases. *Cell.* 1993 Nov 19;75(4):805–816. doi: [10.1016/0092-8674\(93\)90499-G](https://doi.org/10.1016/0092-8674(93)90499-G)